

The complete connectome of a learning and memory centre in an insect brain

Katharina Eichler^{1,2*}, Feng Li^{1*}, Ashok Litwin-Kumar^{3*}, Youngser Park⁴, Ingrid Andrade¹, Casey M. Schneider-Mizell¹, Timo Saumweber⁵, Annina Huser², Claire Eschbach¹, Bertram Gerber^{5,6,7}, Richard D. Fetter¹, James W. Truman¹, Carey E. Priebe⁴, L. F. Abbott^{3,8§}, Andreas S. Thum^{2†§}, Marta Zlatic^{1,9§} & Albert Cardona^{1,10§}

Associating stimuli with positive or negative reinforcement is essential for survival, but a complete wiring diagram of a higher-order circuit supporting associative memory has not been previously available. Here we reconstruct one such circuit at synaptic resolution, the *Drosophila* larval mushroom body. We find that most Kenyon cells integrate random combinations of inputs but that a subset receives stereotyped inputs from single projection neurons. This organization maximizes performance of a model output neuron on a stimulus discrimination task. We also report a novel canonical circuit in each mushroom body compartment with previously unidentified connections: reciprocal Kenyon cell to modulatory neuron connections, modulatory neuron to output neuron connections, and a surprisingly high number of recurrent connections between Kenyon cells. Stereotyped connections found between output neurons could enhance the selection of learned behaviours. The complete circuit map of the mushroom body should guide future functional studies of this learning and memory centre.

Massively parallel, higher-order neuronal circuits such as the cerebellum and insect mushroom body (MB) serve to form and retain associations between stimuli and reinforcement in vertebrates and evolutionarily complex invertebrates^{1–6}. Although these systems provide a biological substrate for adaptive behaviour, no complete synapse-resolution wiring diagram of their connectivity has been available to guide analysis and aid understanding. The MB is a higher-order parallel fibre system in many invertebrate brains, including hemimetabolous as well as holometabolous insects and their larval stages⁶. MB function is essential for associative learning in adult insects^{1,3–5} and in *Drosophila* larvae^{1,7,8}, from the earliest larval stages onwards⁹. Indeed, the basic organization of the adult and the larval MB and their afferent circuits is very similar; however, larvae have about an order of magnitude fewer neurons⁷. Thus, to systematically investigate the organizational logic of the MB, we used serial section electron microscopy to map with synaptic resolution the complete MB connectome in a first-instar *Drosophila* larva (L1; Fig. 1a). L1 are foraging animals capable of all behaviours previously described in later larval stages¹⁰, including adaptive behaviours dependent on associative learning^{7,9} (Fig. 1b). Their smaller neurons enable fast electron microscopy imaging of the entire nervous system and reconstruction of complete circuits^{11,12}.

Models of sensory processing in many neural circuits feature neurons that fire in response to combinations of sensory inputs, generating a high-dimensional representation of the sensory environment¹³. The intrinsic MB neurons, the Kenyon cells (KCs), integrate in their dendrites inputs from combinations of projection neurons (PNs) that encode various stimuli, predominantly olfactory in both adult^{1,4–6} and larva^{12,14}, but also thermal, gustatory, and visual in adult^{5,6,15} and larva

(reported here for the first time, to our knowledge). Previous analyses in adults^{16,17} and larvae¹⁴ suggest that the connectivity between olfactory PNs and KCs is random, but they do not eliminate the possibility of some degree of bilateral symmetry, which requires access to the full PN-to-KC wiring diagram in both hemispheres.

The MB contains circuitry capable of associating reward or punishment with the representation of the sensory environment formed by KCs. KCs have long parallel axons that first run together, forming the peduncle, and then bifurcate, forming the so-called lobes, in both larvae⁷ and adults^{1,4,6,18}. KCs receive localized inputs along their axonal fibres from dopaminergic as well as octopaminergic modulatory neurons (DANs and OANs, respectively) that define separate compartments. DANs and OANs have been shown to convey reinforcement signals in adult insects^{3–6,19–24} and larval *Drosophila*^{7,8}. The dendrites of the mushroom body output neurons (MBONs) respect the DAN compartments in adults^{5,18,25,26} and larvae⁹. It has been shown in adult *Drosophila* that co-activation of KCs and DANs can associatively modulate the KC–MBON synapse^{5,19,20,22,24,26–28}. Thus, the compartments represent anatomical and functional MB units where sensory input (KCs) is integrated with internal reinforcement signals (DANs/OANs) to modulate instructive output for behavioural control (MBONs). However, the synaptic connectivity of KCs, DAN/OANs, and MBONs at this crucial point of integration was previously unknown.

Furthermore, studies in adult *Drosophila* have shown that, despite the compartmental organization of the MB, many MBONs interact with MBONs from other compartments, suggesting that the MBON network functions combinatorially during memory formation and retrieval^{18,25,28}. However, a comprehensive account of all MB neuron

¹Howard Hughes Medical Institute Janelia Research Campus, 19700 Helix Drive, Ashburn, Virginia 20147, USA. ²Department of Biology, University of Konstanz, Universitätsstrasse 10, 78464 Konstanz, Germany. ³Mortimer B. Zuckerman Mind Brain Behavior Institute, Department of Neuroscience, Columbia University, 3227 Broadway, New York, New York 10027, USA. ⁴Department of Applied Mathematics and Statistics, Whiting School of Engineering, Johns Hopkins University, 100 Whitehead Hall, 3400 North Charles Street, Baltimore, Maryland 21218, USA. ⁵Abteilung Genetik von Lernen und Gedächtnis, Leibniz Institut für Neurobiologie, 39118 Magdeburg, Germany. ⁶Otto-von-Guericke Universität Magdeburg, Institut für Biologie, Verhaltensgenetik, Universitätsplatz 2, D-39106 Magdeburg, Germany. ⁷Otto-von-Guericke University Magdeburg, Center for Behavioral Brain Sciences, Universitätsplatz 2, D-39106 Magdeburg, Germany. ⁸Department of Physiology and Cellular Biophysics, Columbia University, Russ Berrie Pavilion, 1150 St Nicholas Avenue, New York, New York 10032, USA. ⁹Department of Zoology, University of Cambridge, Downing Street, Cambridge CB2 3EJ, UK. ¹⁰Department of Physiology, Development and Neuroscience, University of Cambridge, Downing Street, Cambridge CB2 3DY, UK. [†]Present address: Department of Genetics, University of Leipzig, Talstrasse 33, 04103 Leipzig, Germany.

*These authors contributed equally to this work.

§These authors jointly supervised this work.

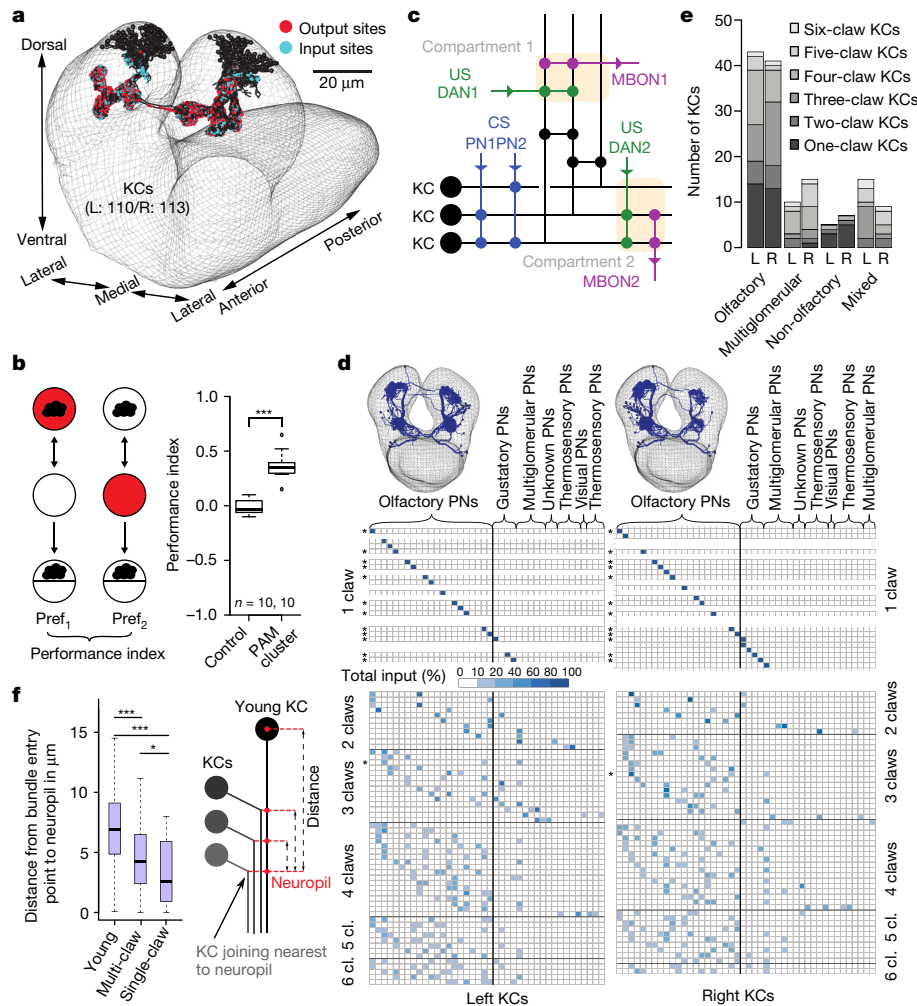


Figure 1 | Mushroom bodies of a first-instar *Drosophila* larva.

a, KCs from an electron microscopy volume of the whole central nervous system. **b**, Associative learning in first-instar larvae: in a Petri dish, we presented an odour (cloud) and red light, either paired (left) or unpaired (right), and computed the performance index. Control larvae (attP2;UAS-CsChrimson) receiving paired stimuli did not learn, whereas larvae in which optogenetic activation of dopaminergic (PAM cluster) neurons (GMR58E02-GAL4;UAS-CsChrimson) was paired with odour showed robust appetitive learning ($P < 0.0001$). **c**, Diagram of the literature's MB circuitry model. PN relay sensory stimuli to KC dendrites. MBON dendrites and MBIN (DAN, OAN, and other) axons tile the parallel KC axons, defining compartments (coloured boxes). MBINs signal reward or punishment, and KCs synapse onto output neurons (MBONs). **d**, PN-to-KC connectivity, colour-coded by percentage of inputs on KC dendrites.

Uniglomerular olfactory PNs (Olfactory PNs) and other PNs synapse onto single-claw or multi-claw KCs. Stars indicate KCs with identical input patterns on the left and right hemispheres. For the PNs on the right of the black vertical lines, the first 18 columns are left–right homologous PNs, the last column (left) and last five columns (right) are hemisphere-specific PNs. **e**, Number of KCs integrating inputs from uniglomerular olfactory PNs, multiglomerular olfactory PNs, non-olfactory PNs, or a mixture of these PN types. L, left; R, right. **f**, Earlier-born KCs join the lineage bundle closer to the neuropil surface than later-born ones, meaning older KCs present fewer claws than younger ones. Distances span from the point where the KC joins the bundle to the joining point of the KC nearest to the neuropil. Differences between all groups are significant ($***P < 0.0001$; single-claw and multi-claw KC comparison $P = 0.0237$).

connections is lacking. Thus, to provide a basis for understanding how the MB, a prototypical parallel fibre learning and memory circuit, functions as an integrated whole, we provide a full, synapse-resolution connectome of all MB neurons of an L1 *Drosophila* larva.

Results

We reconstructed all the KCs in both brain hemispheres of an L1 *Drosophila* larva and identified all of their pre- and postsynaptic partners. We found 223 KCs (110 on the left, 113 on the right), of which 145 were mature (73 on the left, 72 on the right). Immature KCs either lack or have tiny dendrites, and their axons terminate early with filopodia typical of axon growth cones. Every mature KC presents a well-developed dendrite, and its axon innervates all of the MB compartments. Although the number of KCs was different between the two sides (Fig. 1a), we found exactly 24 MBONs, 7 DANs, 2 paired and 2 unpaired OANs, and 5 additional modulatory input neurons (which

we call MBINs or mushroom body input neurons, a term we also use to refer to all the modulatory neurons collectively) of unknown neurotransmitter identity (Supplementary Fig. 1a and Supplementary Table 3). An additional pair of GABAergic neurons, homologous to the anterior paired lateral (APL) neurons in the adult fly^{29,30}, synapses reciprocally with all mature ipsilateral KCs (Extended Data Fig. 1).

PN inputs to the KCs

We identified all the sensory PNs and their connections onto KCs. KC dendrites have claw-like structures that wrap around PN axon boutons in the MB calyx⁶ (Extended Data Fig. 2b). We identified input from 21 uniglomerular olfactory PNs on each side¹², 5 and 7 multiglomerular PNs¹², and 14 and 16 non-olfactory PNs on the left and right sides, respectively. Non-olfactory PNs include thermal, gustatory, mixed olfactory, and possibly other modalities (Fig. 1d, e and Supplementary Table 1). A subset of mature KCs receive input from only

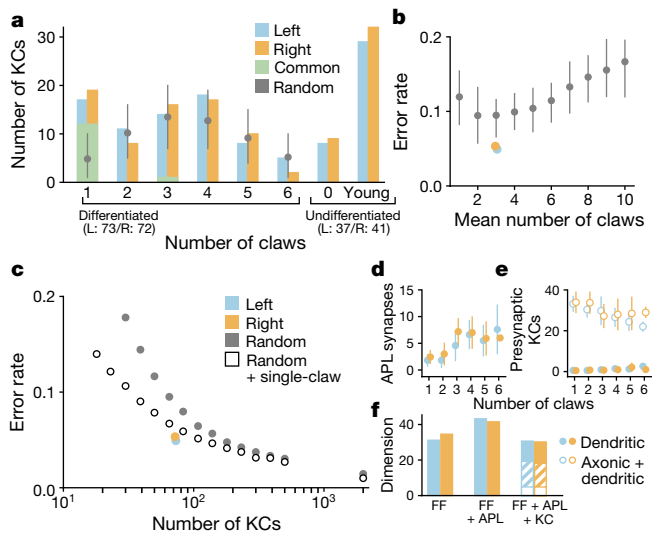


Figure 2 | KC connectivity reduces redundancy and optimizes stimulus discrimination. **a**, Distribution of KC claw numbers compared with random models. Random models have significantly fewer single-claw KCs ($P < 10^{-5}$). Grey circles and lines denote mean and 95% confidence intervals. **b**, Classification error rate of a readout of the KC representation trained on a stimulus discrimination task. Observed connectivity (blue and orange) is compared with random models (grey) in which KCs have different distributions of average claw numbers. In **a** and **b**, grey circles and lines denote mean and 95% confidence intervals for random models. **c**, Average performance of models with purely random connectivity (grey) or random multi-claw plus non-random single-claw KCs (white). Standard error of the mean is smaller than the marks. **d**, Number of APL-to-KC synapses, which is correlated with claw number. **e**, Number of presynaptic KC-to-KC connections, which is inversely related to postsynaptic claw number. Dendro-dendritic (filled circles) or all synapses (open circles) are shown. In **d** and **e**, coloured circles and lines denote mean \pm s.e.m. from the reconstructed data. **f**, Dimension of KC representation in models with only feedforward PN-to-KC connections (FF), with APL-mediated inhibition (FF + APL), or with inhibition and excitatory KC-to-KC connections (FF + APL + KC). Dimension is slightly reduced by dendritic KC-to-KC connections (right, filled bars) but strongly reduced by axonic KC-to-KC connections (open bars). Facilitatory axonic KC-to-KC connections (hatched bars) yield an intermediate reduction.

one PN (single-claw KCs), while the remaining KCs (multi-claw KCs, as in the adult fly¹⁷) receive input from two to six PNs¹⁴ (Fig. 1d and Extended Data Fig. 2c). Notably, single-claw KCs are born earlier than multi-claw KCs (Fig. 1f). KCs with different numbers of claws receive roughly the same number of synapses summed across claws (Extended Data Fig. 2a). This suggests that multi-claw KCs may require input from multiple PNs to respond, assuring combinatorial selectivity^{31,32}.

Two features of the PN-to-KC connectivity are immediately visible (Fig. 1d): the contrast between the ordered and apparently disordered connections onto single-claw KCs and multi-claw KCs, respectively, and the existence of KCs that do not receive any uni-glomerular PN input. Most KCs (77%) receive exclusively olfactory input from uni- or multi-glomerular PNs, while the others receive non-olfactory input (Fig. 1d, e). Prominent among these are two KCs per side that exclusively receive thermal information. No structure is apparent in the olfactory PN input to multi-claw KCs (Fig. 1d; see Extended Data Fig. 3b–e for further analysis), consistent with previous analyses in adults^{16,17} and larvae¹⁴. Structure was found, however, when all the PNs were included in the analysis, reflecting the presence of specialized non-olfactory KCs (Extended Data Fig. 3a). We also determined that PN connections onto multi-claw KCs in the left and right hemispheres are statistically independent. Only one bilateral pair of multi-claw KCs receives input from the same set of homologous PNs (marked by asterisks in Fig. 1d), no more than predicted by a random model ($P = 0.52$; Extended Data Fig. 3e). Such asymmetry has

not been observed previously in the L1, where strongly connected presynaptic partners of identified neurons have always been seen to have left and right homologues^{11,12}.

In contrast to the randomness of multi-claw KCs, the number of single-claw KCs is significantly greater than predicted by random models (Fig. 2a), and Fig. 1d shows clear structure in their wiring. If single-claw KCs sampled random PNs, we would expect to find about five pairs of single-claw KCs innervated by the same PN per hemisphere ('duplicates'). The data indicate zero left-hemisphere and one right-hemisphere duplicate ($P < 0.002$ and $P < 0.005$ in the random model, respectively). By contrast, the random model predicts that duplicates should be rare for multi-claw KCs, and the data reveal only two ($P = 0.93$). The fact that single-claw KCs appear earliest in development suggests that a top priority, initially, is to assure that a complete set of signals is relayed to the MBONs, which is not guaranteed with random wiring. Indeed, we calculated that 27 (left) and 44 (right) randomly wired multi-claw KCs, on average, would be needed to achieve the same level of coverage of PN inputs as the 17 (left) and 19 (right) single-claw KCs (Methods).

PN-to-KC connectivity optimizes associative learning

The lack of duplication in PN-to-KC connections suggests that MB wiring is well suited to promote KC diversity. We hypothesized that this diversity produces a high-dimensional odour representation that supports stimulus classification. To test this idea, we developed a model in which KCs produce sparse responses to random combinations of odour-evoked PN activity (Methods). We compared the performance on a stimulus classification task of a model MBON in networks with the observed PN-to-KC connectivity and completely randomly connected models with varying degrees of connectivity (see Methods). Fully random networks have few of the single-claw KCs observed in the reconstruction (Fig. 2a).

The observed connectivity leads to performance superior to the average of purely random model networks (Fig. 2b). Motivated by the observation that unique single-claw KCs are born early in MB development (Fig. 1f), we hypothesized that their presence may be particularly important when the number of KCs is small. We therefore compared the performance of networks with only randomly connected KCs to that of networks with the same total number of KCs but containing a subpopulation of unique single-claw KCs. In networks with few KCs, the presence of single-claw KCs substantially improves performance (Fig. 2c). As additional KCs are added, the advantage of single-claw KCs diminishes. For networks constructed using estimates of adult *Drosophila* KC connectivity, where single-claw KCs have not been identified¹⁷, unique single-claw KCs provide only a small benefit.

Inhibitory KC interactions via the APL neuron

The MB is innervated by the GABAergic (γ -aminobutyric-acid-releasing) APL neuron in the adult fly²⁹ and in the larva³⁰. APL synapses reciprocally with all mature KCs (Extended Data Fig. 1a). Although APL receives most of its input from multi-claw KCs, individual single-claw KCs typically have more synapses onto APL dendrites than multi-claw KCs (Extended Data Fig. 1b, c). Conversely, APL connects more strongly to KCs with more claws (Fig. 2d and Extended Data Fig. 1c). We extended our model to include APL-mediated feedback inhibition and assessed its effect on the dimension of the KC representation. The dimension quantifies the level of decorrelation of KC responses and is related to their ability to support stimulus classification³³ (Fig. 2b, c; see Methods). The addition of recurrent APL inhibition increases the dimension by approximately 30% (Fig. 2f), consistent with the proposed role of APL in maintaining sparse, decorrelated KC responses^{30,34,35}. The increased inhibition received by multi- compared with single-claw KCs might reflect a greater need for decorrelation of their responses given the larger overlap of their PN inputs.

Recurrent KC interactions

We next examined whether KCs directly interact with each other, a possibility suggested by previous studies in *Drosophila* and other species⁶. We found that, on average, 60% of the synapses received by KCs come from other KCs and 45% of KC output synapses are onto other KCs (Fig. 2e and Extended Data Fig. 2d–g). Most KC-to-KC synapses are axo-axonic and located in the peduncle and MB lobes; a much smaller fraction are dendro-dendritic and located in the calyx (Extended Data Fig. 2h). The largest number of KC-to-KC connections occurs between the two thermosensory KCs (Supplementary Table 1), but these KCs also make large numbers of connections to olfactory and visual KCs. Single-claw KCs make more recurrent connections, on average, than multi-claw KCs, and both single- and multi-claw KCs tend to connect reciprocally to KCs of the same type (Extended Data Fig. 4a–g). However, we found no relationship between the similarity of the PN inputs to KC pairs and the number of KC-to-KC synapses formed between them (correlation coefficients 0.006 and -0.02 for left and right hemispheres; $P > 0.3$, compared with shuffled network).

KCs have been shown to be cholinergic in the adult³⁶, so it is likely that KC-to-KC connections are depolarizing. When strong dendro-dendritic KC connections are added to our model, dimension only decreases slightly (Fig. 2f). Additional subthreshold facilitatory axo-axonic KC-to-KC connections also have a weak effect (Fig. 2f, hatched bars). However, if the axo-axonic connections we model are stronger, the dimension collapses because of the large correlations introduced by this recurrence (Fig. 2f, open bars). Although our model does not reveal a functional role for KC-to-KC connections, it is possible that processes that we did not model, such as experience-dependent modulation of their synaptic strengths, may modify the representation to favour either behavioural discrimination or generalization³⁷. Further characterization of these connections is needed to assess this hypothesis.

MBINs and MBONs

We next identified the MBONs and modulatory neurons (MBINs) associated with every MB compartment (Fig. 3a). Each compartment is innervated by one to five MBONs and one to three MBINs (most often DANs and OANs), except for the shaft compartment of the medial lobe which lacks MBINs in L1 larvae (but has them in L3 (ref. 8)). Most MBONs and MBINs innervate a single MB compartment (although most MBINs present a bilateral axon, innervating both the left and right homologous compartments), with few exceptions (MBIN-11 and 5/24 MBONs; Fig. 3d and Extended Data Fig. 5). Most MBINs (over 80%) are primarily presynaptic to other MB neurons, but some allocate 50% or more of their outputs to non-MB neurons (Extended Data Fig. 6a and Supplementary Table 2b). We also found that larger MBIN axons make more synapses onto KCs, and likewise for KC synapses onto larger MBON dendrites (Extended Data Fig. 6b, c).

Antibody labelling of green fluorescent protein (GFP)-labelled neurons showed that seven MBINs are dopaminergic (DAN-c1, -d1, -f1, -g1, -i1, -j1, and -k1; Extended Data Fig. 5), four are octopaminergic (OAN-a1, -a2, -e1, and -g1), three others are neither dopaminergic nor octopaminergic (MBIN-e1, -e2, and -11), and two were not technically accessible (MBIN-b1 and -b2) (Supplementary Fig. 2a). MBONs are glutamatergic, cholinergic, or GABAergic (Supplementary Fig. 2b), the same set of neurotransmitters seen for adult MBONs¹⁸ (Supplementary Table 3).

A canonical circuit motif in each MB compartment

Electron microscopy reconstruction of MBONs and MBINs revealed a canonical circuit motif (Fig. 3b, d and Extended Data Fig. 5) that appears in every compartment, independent of MBIN or MBON neurotransmitters (except in the shaft compartment lacking modulatory input in L1). In this motif, KCs synapse onto MBONs, as previously shown in adult *Drosophila*^{5,6,24,36} and bees and locusts^{3,6,38}. However, we identified two unexpected connection types. The first are numerous KC-to-MBIN connections (Fig. 3d and Extended Data Fig. 5). Second,

a sizeable fraction of MBIN presynaptic sites (which are polyadic) simultaneously contacts both KCs and MBONs, with generally at least one of the postsynaptic KCs synapsing onto one of the postsynaptic MBONs within less than a micrometre of the MBIN–KC synapse (Fig. 3c). Thus, MBINs synapse onto both the pre- and postsynaptic sides of many KC-to-MBON synapses. For comparison, MBONs receive on average 3.44% of their input from individual MBINs and 1.3% from an individual KC. If 5% of the 73 mature KCs are active in response to a given odour, as has been shown in the adult³¹, then the MBONs receive on average about 4.8% of their input from active KCs, very similar to the percentage of MBIN input.

MBINs convey reinforcement signals and are thought to modulate the efficacy of KC-to-MBON connections through volume release in the vicinity of KC presynaptic terminals^{1,3–6,24–27} and, as expected, we observed MBIN axon boutons containing dense-core vesicles (Extended Data Fig. 7). We also observed dense-core vesicles in addition to clear-core vesicles in one-third of KCs (Extended Data Fig. 7), consistent with findings in the adult that many KCs co-release short neuropeptide F (sNPF) with acetylcholine³⁶.

Our electron microscopy reconstruction also revealed MBIN synapses containing clear vesicles (Extended Data Fig. 7 and Fig. 3c) indistinguishable from those that release classical neurotransmitters¹¹. All MBIN terminals with clear-core vesicles contained dense-core vesicles, mostly within presynaptic boutons (Extended Data Fig. 8). This suggests that MBINs may have two concurrent modes of action onto KCs and MBONs: activation via synaptic release (of dopamine, octopamine, or fast neurotransmitters³⁹) and neuromodulation via volume release. These two modes, coupled with the diverse connection types among KCs, MBINs, and MBONs, may provide a powerful and flexible substrate for associative learning.

Heterogeneous KC-to-MBON/MBIN connections

Previous studies in adult *Drosophila* have shown that different lobes and compartments within the lobes are involved in forming different types of memory^{1,4,5,19–22,25,26,28,40,41}. Functional studies in larvae^{8,42} also suggest that vertical and medial lobes may be implicated in distinct types of memory formation (aversive and appetitive, respectively). Our electron microscopy study shows that all mature KCs make synaptic connections with MBONs and MBINs (DANs, OANs, and others) in both the vertical and medial MB lobes (Extended Data Figs 9a–c and 10a–c and Supplementary Table 4a, b). Furthermore, individual MBONs are innervated by between 40% and almost all of the KCs, with an average of 70% (Extended Data Fig. 9a). This extensive innervation provides MBONs access to the high-dimensional KC representation and suggests that individual KCs may be involved in the formation and storage of associations involving multiple stimuli and valences, as suggested for the adult^{1,4,5} (but see ref. 43).

Our electron microscopy reconstruction reveals that, in the larva, the axon terminals of all MBINs overlap with all KCs within a compartment and could potentially connect to all KCs, unlike in the adult^{18,43}. Nevertheless, only subsets of KCs synapse onto either the MBIN or the MBON, or both, within a given compartment, with a broad distribution in the number of synaptic contacts (Extended Data Figs 9d, e and 10d, e and Supplementary Table 4a, b). Estimating connection strength using synapse number, distinct subsets of KCs synapse strongly with MBINs and MBONs in distinct compartments (Extended Data Figs 9c and 10c and Supplementary Tables 1 and 4a, b). This could arise from an innately broad distribution of synapse strengths or activity-dependent changes in synapse number. Either way, this heterogeneity implies that distinct MBONs and MBINs respond to heterogeneous combinations of active KCs.

Comprehensive profile of MBON inputs

Electron microscopy reconstruction and synaptic counting provides a comprehensive view of the signals carried by the MBONs (Fig. 4a, b and Supplementary Table 2a). In general, MBONs are among the

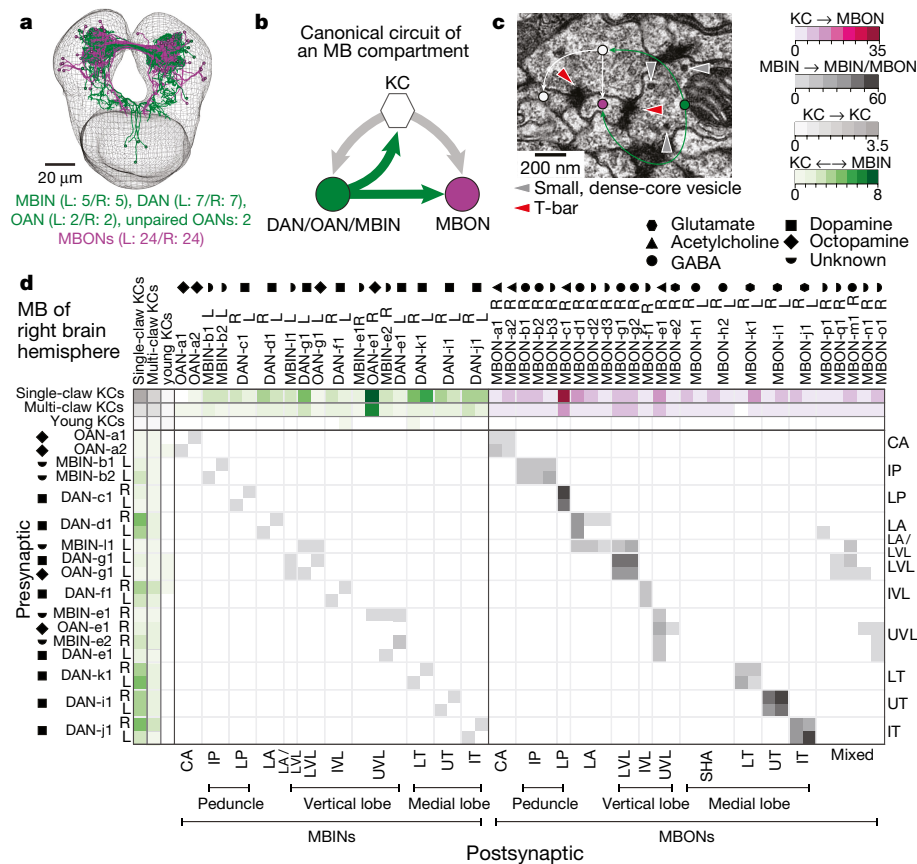


Figure 3 | A canonical circuit in every MB compartment. **a**, Electron microscopy-reconstructed DAN/OAN/MBINs (green) and MBONs (magenta). **b**, Canonical circuit present in every MB compartment, with previously unknown KC synapses onto MBINs (DAN, OAN, and others), and from these onto MBONs. **c**, Example of an MBIN (green dot) synapse with a KC (white dot) and an MBON (magenta dot). The same KC is also presynaptic to the MBON in close proximity. Dense- and clear-core vesicles are present near the DAN presynaptic site. **d**, The connectivity matrix between KCs, DAN/OAN/MBINs, and MBONs of

the right-hemisphere MB shows specific, compartment-centric synapses among cells types. Each entry represents the number of synapses from a row to a column (values are averaged for KCs). Note the absence of DAN in SHA (develops later in larval life). DAN/OAN/MBINs synapse only onto MBONs innervating their compartment, and axo-axonically onto same-compartment DAN/OAN/MBINs. Note multi-compartment MBONs in the vertical lobe and lateral appendix (LA). CA, calyx; IP, intermediate peduncle; LP, lower peduncle; LT, lower toe; UT, upper toe; IT, intermediate toe.

neurons in the L1 larval brain receiving the largest number of inputs, with a median of 497 and a maximum of about 1,500 postsynaptic sites. The median for other neurons reconstructed so far is around 250 in L1 (refs 11, 12).

We analysed the detailed structure of KC-to-MBON connectivity to determine the nature of the sensory signals relayed to MBONs. About 23% of the KC input to MBONs originates in KCs that integrate inputs from non-olfactory PNs (Fig. 4b, c), significantly more than in networks with shuffled PN modalities ($P < 0.05$). This pattern of non-olfactory input is stereotyped: the fraction of non-olfactory input received by homologous MBONs across hemispheres is more similar than across different MBONs in the same hemisphere ($P < 0.001$, Mann–Whitney U -test). These observations, along with the sparse activity of olfactory KCs seen in adult flies³¹, suggest that non-olfactory signals may have a large influence on the activity of certain MBONs despite the small number of non-olfactory KCs. To quantify this influence for one modality, we compared the total number of synapses made by thermosensory KCs onto the different MBONs to 0.05 times the total number of synapses made by non-thermosensory KCs (Extended Data Fig. 9f). This ratio quantifies the relative influence of a stimulus that activates thermosensory KCs to a typical odour stimulus that activates 5% of olfactory KCs³¹. The ratio is high for some MBONs (-d3, -o1, and -b3) and stereotyped for homologous MBONs across hemispheres, suggesting that these MBONs may be wired to respond strongly to non-olfactory cues, such as temperature.

We also examined whether the olfactory input received by homologous MBONs is stereotyped by computing the correlation between the number of connections they receive from each olfactory PN via KCs. Unlike for non-olfactory input, homologous MBONs across hemispheres receive a less similar pattern of olfactory PN input than different MBONs in the same hemisphere ($P > 0.99$, Mann–Whitney U -test), arguing against stereotypy. Therefore the lack of stereotypy in the olfactory PN-to-KC connectivity and the greater degree of stereotypy in the non-olfactory PN-to-KC connectivity are inherited by the MBONs.

Notably, MBONs do not receive their inputs exclusively from KCs, DANs, and other MBONs. We found that some compartments (Fig. 4b) have two kinds of MBONs that differ in the amount of input they receive from non-MB sources. Some MBONs are postsynaptic almost exclusively to MB neurons (over 90%), while some receive 50% or more of their inputs from non-MB neurons on dendritic branches outside the MB compartments (Fig. 4b and Supplementary Table 2a). MBONs with significant input from outside the MB typically receive input from other MBONs as well. The convergence of modulatory neurons, of olfactory, thermal, and visual KCs, and of non-MB inputs onto some MBONs suggests they may be flexible sites for learning and integration of multisensory and internal state information (via DANs, as suggested by functional studies in the adult^{19,28,44,45}, and possibly via the other new non-MB inputs identified here).

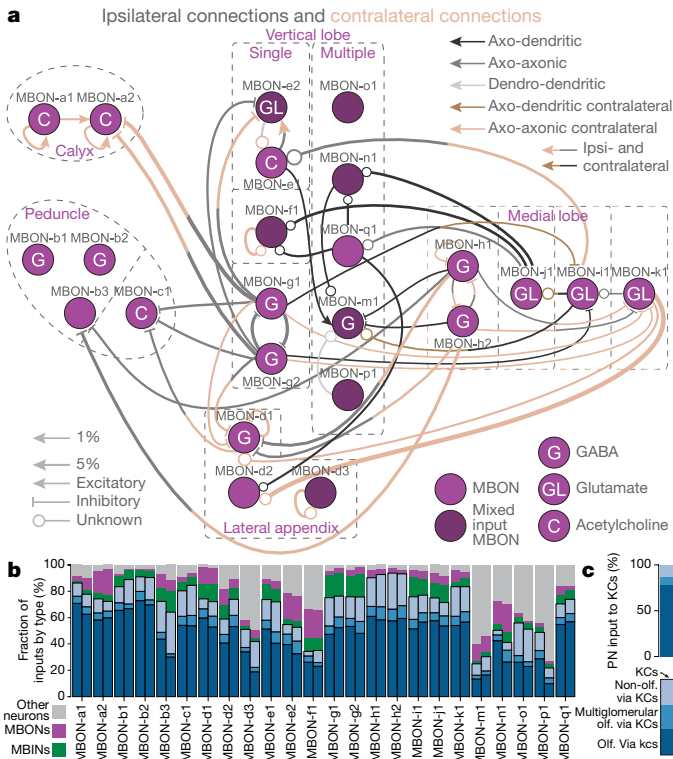


Figure 4 | MBON inputs and circuits. **a**, MBONs are in the compartments innervated by their dendrites. Most connections among MBONs are axo-axonic, and fewer are axo-dendritic. Few MBONs avoid synapsing to others. Most inter-lobe connections are mediated by GABAergic (MBON-g1, -g2, -h1, -h2) and glutamatergic (MBON-i1, -j1, -k1) MBONs, potentially providing a substrate for lateral inhibition between compartments of opposite valence. **b**, Fraction of MBON inputs by neuron type. Left and right homologous MBONs are shown adjacent. Only some vertical lobe and lateral appendix MBONs get less than 80% of their input from MB neurons and less than 60% from KCs. Almost all multi-compartment MBONs (MBON-m1, -n1, -o1 and -p1) have a higher fraction of input from non-MB neurons than single-compartment MBONs. The fraction of inputs from PNs to MBONs via KCs is shown within the fraction of KC input (different shades of blue), computed by the product of the PN-to-KC and KC-to-MBON connections. Most MBONs receive a high fraction of olfactory input via KCs while few MBONs (-b3, -o1) get nearly half of their inputs via KCs from non-olfactory PNs. **c**, Percentages of different types of PN input to the KCs. While there are almost equal numbers of olfactory (olf.) and non-olfactory PNs synapsing onto KCs, non-olfactory PNs represent only about 12% of the inputs to KC dendrites.

The MBON output network

In adult *Drosophila*, MBONs form a multi-layered feedforward network^{18,28}. Consistent with this, we found synaptic connections between MBONs in different compartments, on both the ipsi- and contralateral sides, that create a bilaterally symmetric structured feedforward circuit (Fig. 4a and Supplementary Table 5). Most inter-lobe connections are mediated by GABAergic (MBON-g1, -g2, -h1, -h2) and glutamatergic (MBON-i1, -j1, -k1) MBONs, potentially providing a substrate for lateral inhibition between the lobes. Glutamate has previously been found to be inhibitory in the fly⁴⁶, but an excitatory effect on some neurons cannot be excluded. Some vertical lobe MBONs could also disinhibit (via inhibition of inhibitory medial lobe MBONs), or directly excite other vertical lobe MBONs, potentially providing within-region facilitation.

In addition, there is a hierarchy of interactions across regions of the MB. MBONs of the peduncle and calyx are exclusively at the bottom of the inhibitory hierarchy, receiving inputs from GABAergic MBONs from both the vertical lobe and the medial lobe, but not synapsing onto any other MBONs (Fig. 4a). Furthermore, the medial lobe may

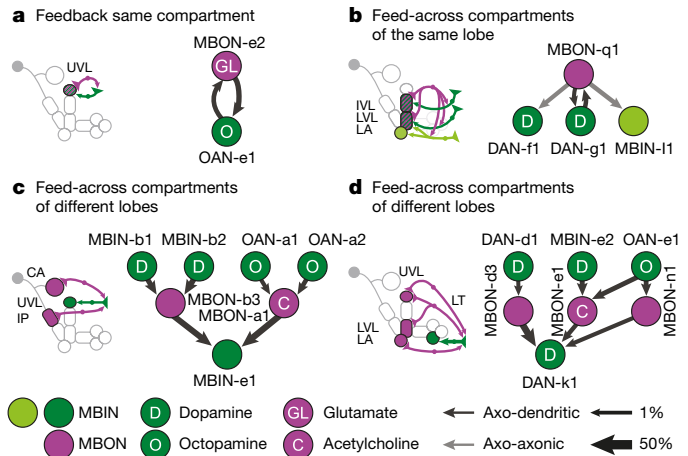


Figure 5 | Intra- and inter-compartment feedback: MBONs of one MB compartment synapse onto MBINs of the same or other compartments. Schematics of connections from output neurons (MBONs) onto input neurons (MBINs) within their own (feedback) or into other (feed-across) compartments. **a**, The output neuron MBON-e2 synapses onto the dendrites of OAN-e1 in its own compartment, UVL. **b**, Feedback among compartments of the same lobe suggests that the establishment of a memory in a compartment can affect the DANs of adjacent compartments. **c**, Feed-across motif from proximal MB compartments (calyx and intermediate peduncle) to a distal one (UVL). **d**, Feed-across motif from the vertical lobe to the medial lobe.

also disinhibit the peduncle MBON-c1 that the vertical lobe inhibits (Fig. 4a).

MBON connections to MBINs

The MB connectome further reveals several feedback connections from MBONs onto MBINs of the same compartment (Fig. 5a, b). MBON-e2 from the tip compartment of the vertical lobe (UVL) synapses onto the dendrites of OAN-e1 outside the MB (bilateral; Fig. 5a and Supplementary Fig. 1b). MBON-q1 from the intermediate (IVL) and lower vertical lobe (LVL) compartments is presynaptic to the axons of the DANs from these two compartments in addition to the MBIN-11 from the lateral appendix compartment (Fig. 5b and Supplementary Fig. 1b). An MBON-to-DAN feedback connection was found in the α1 compartment of the adult vertical lobe and is implicated in the formation of long-term memory²³.

Notably, we also found hetero-compartment feed-across connections where MBONs innervating one region of the MB synapse onto MBINs innervating other regions (Fig. 5c, d and Supplementary Fig. 1b). The feed-across motifs could play a role during conflicting memory formation^{20,41} or during reversal learning, and more generally they could enhance the flexibility of modulatory input to the MB.

Discussion

We provide the first complete wiring diagram of a parallel fibre circuit for adaptive behavioural control. Such circuits exist in various forms, for example the cerebellum in vertebrates and the MB in insects. They contribute to multiple aspects of behavioural control including stimulus classification, the formation and retrieval of Pavlovian associations, and memory-based action selection¹⁻⁹. A comprehensive wiring diagram of such a multi-purpose structure is an essential starting point for functionally testing the observed structural connections and for elucidating the circuit implementation of these fundamental brain functions.

Even though individual neurons may change through metamorphosis, many of the basic aspects of the MB architecture are shared between larval and adult *Drosophila* stages and with other insects (see Supplementary Tables 6 and 7)^{1,3-6,8,18,39,40}. We therefore expect that the circuit motifs identified here are not unique to the L1 developmental stage, but instead represent a general feature of *Drosophila* and insect MBs.

A canonical circuit in each MB compartment

Our electron microscopy reconstruction revealed a canonical circuit in each MB compartment featuring two unexpected motifs in addition to the previously known MBIN-to-KC and KC-to-MBON connections. First, we were surprised to observe that the number of KC-to-MBIN and KC-to-MBON synapses are comparable. As KCs were shown to be cholinergic in adults³⁶, KC-to-MBIN connections could be potentially depolarizing. Untrained, novel odours can activate DANs in adult *Drosophila*^{47,48} and OANs in bees³. Similar brief short-latency activations of dopamine neurons by novel stimuli are observed in monkeys, too, and are interpreted as salience signals⁴⁹. Learning could potentially modulate the strength of the KC-to-MBIN connection, either weakening it or strengthening it. The latter scenario could explain the increase in DAN activation by reinforcement-predicting odours observed in adult *Drosophila*⁴⁷, bees, and monkeys^{3,49}. In addition, dopamine receptors have been shown to be required in *Drosophila* KCs for memory formation⁴. Another unexpected finding was that MBINs synapse directly onto MBONs, rather than only onto KCs. Such a motif could provide a substrate for neuromodulator-gated Hebbian spike-timing dependent plasticity, which has been observed in the locust MB³⁸.

Dimensionality of the KC representation

In addition to random and bilaterally asymmetric olfactory and structured non-olfactory PN-to-KC connectivity (Extended Data Fig. 3), our analysis identified single-claw KCs whose number and lack of redundancy are inconsistent with random wiring (Fig. 2). Random wiring has previously been shown to increase the dimension of sensory representations when the number of neurons participating in the representation is large compared with the number of afferent fibres, as in the cerebellum or adult MB^{13,33}. However, our model shows that when the number of neurons is limited, random wiring alone is inferior to a combination of random and structured connectivity that ensures each input is sampled without redundancy. The presence of single-claw KCs may reflect an implementation of such a strategy. In general, our results are consistent with a developmental program that produces complete and high-dimensional KC sensory representations to support stimulus discrimination at both larval and adult stages.

Mutual inhibition in the MBON–MBON network

This study reveals the complete MBON–MBON network at synaptic resolution (Fig. 4a). Previous studies in the larva have shown that odour paired with activation of medial and vertical lobe DANs leads to learned approach⁸ and avoidance^{7,42}, respectively. Our connectivity analysis reveals that glutamatergic MBONs from the medial lobe laterally connect to MBONs of the vertical lobe. The glutamatergic MBON–MBON connections could be inhibitory⁴⁶, although further studies are needed to confirm this. Furthermore, inhibitory GABAergic MBONs from the vertical lobe laterally connect to MBONs of the medial lobe. An example is the feedforward inhibition of medial lobe MBON-i1 output neuron by the vertical lobe GABAergic MBON-g1, -g2 output neurons. A similar motif has been observed in the *Drosophila* adult, where aversive learning induces depression of conditioned odour responses in the approach-promoting MBON-MVP2 (MBON-11), which in turn disinhibits conditioned odour responses in the avoidance-promoting MBON-M4/M6 (MBON-03) because of the MBON-MVP2 to MBON-M4/M6 feedforward inhibitory connection^{18,25–28,40}.

Combining the present connectivity analysis of the MBON–MBON network in the larva and previous studies in the adult *Drosophila*^{5,18,25,28,40}, the rule seems to be that MBONs encoding opposite learned valence laterally inhibit each other. Such inhibitory interactions have been proposed as a prototypical circuit motif for memory-based action selection⁵⁰.

Online Content Methods, along with any additional Extended Data display items and Source Data, are available in the online version of the paper; references unique to these sections appear only in the online paper.

Received 20 July 2016; accepted 4 July 2017.

- Heisenberg, M. Mushroom body memoir: from maps to models. *Nat. Rev. Neurosci.* **4**, 266–275 (2003).
- Farris, S. M. Are mushroom bodies cerebellum-like structures? *Arthropod Struct. Dev.* **40**, 368–379 (2011).
- Menzel, R. The honeybee as a model for understanding the basis of cognition. *Nat. Rev. Neurosci.* **13**, 758–768 (2012).
- Waddell, S. Reinforcement signalling in *Drosophila*; dopamine does it all after all. *Curr. Opin. Neurobiol.* **23**, 324–329 (2013).
- Owald, D. & Waddell, S. Olfactory learning skews mushroom body output pathways to steer behavioral choice in *Drosophila*. *Curr. Opin. Neurobiol.* **35**, 178–184 (2015).
- Schürmann, F.-W. Fine structure of synaptic sites and circuits in mushroom bodies of insect brains. *Arthropod Struct. Dev.* **45**, 399–421 (2016).
- Diegelmann, S., Klagges, B., Michels, B., Schleyer, M. & Gerber, B. Maggot learning and synapsin function. *J. Exp. Biol.* **216**, 939–951 (2013).
- Rohwedder, A. *et al.* Four individually identified paired dopamine neurons signal reward in larval *Drosophila*. *Curr. Biol.* **26**, 661–669 (2016).
- Pauls, D., Selcho, M., Gendre, N., Stocker, R. F. & Thum, A. S. *Drosophila* larvae establish appetitive olfactory memories via mushroom body neurons of embryonic origin. *J. Neurosci.* **30**, 10655–10666 (2010).
- Almeida-Carvalho, M. J. *et al.* The Ollmpiad: concordance of behavioural faculties of stage 1 and stage 3 *Drosophila* larvae. *J. Exp. Biol.* **220**, 2452–2475 (2017).
- Ohyama, T. *et al.* A multilevel multimodal circuit enhances action selection in *Drosophila*. *Nature* **520**, 633–639 (2015).
- Berck, M. E. *et al.* The wiring diagram of a glomerular olfactory system. *eLife* **5**, e14859 (2016).
- Babadi, B. & Sompolinsky, H. Sparseness and expansion in sensory representations. *Neuron* **83**, 1213–1226 (2014).
- Masuda-Nakagawa, L. M., Tanaka, N. K. & O’Kane, C. J. Stereotypic and random patterns of connectivity in the larval mushroom body calyx of *Drosophila*. *Proc. Natl Acad. Sci. USA* **102**, 19027–19032 (2005).
- Bang, S. *et al.* Dopamine signalling in mushroom bodies regulates temperature-preference behaviour in *Drosophila*. *PLoS Genet.* **7**, e1001346 (2011).
- Murthy, M., Fiete, I. & Laurent, G. Testing odor response stereotypy in the *Drosophila* mushroom body. *Neuron* **59**, 1009–1023 (2008).
- Caron, S. J., Ruta, V., Abbott, L. F. & Axel, R. Random convergence of olfactory inputs in the *Drosophila* mushroom body. *Nature* **497**, 113–117 (2013).
- Aso, Y. *et al.* The neuronal architecture of the mushroom body provides a logic for associative learning. *eLife* **3**, e04577 (2014).
- Lin, S. *et al.* Neural correlates of water reward in thirsty *Drosophila*. *Nat. Neurosci.* **17**, 1536–1542 (2014).
- Das, G. *et al.* *Drosophila* learn opposing components of a compound food stimulus. *Curr. Biol.* **24**, 1723–1730 (2014).
- Galili, D. S. *et al.* Converging circuits mediate temperature and shock aversive olfactory conditioning in *Drosophila*. *Curr. Biol.* **24**, 1712–1722 (2014).
- Huetteroth, W. *et al.* Sweet taste and nutrient value subdivide rewarding dopaminergic neurons in *Drosophila*. *Curr. Biol.* **25**, 751–758 (2015).
- Ichinose, T. *et al.* Reward signal in a recurrent circuit drives appetitive long-term memory formation. *eLife* **4**, e10719 (2015).
- Cohn, R., Morante, I., Ruta, V. Coordinated and compartmentalized neuromodulation shapes sensory processing in *Drosophila*. *Cell* **163**, 1742–1755 (2015).
- Owald, D. *et al.* Activity of defined mushroom body output neurons underlies learned olfactory behavior in *Drosophila*. *Neuron* **86**, 417–427 (2015).
- Bouzaiane, E., Trannoy, S., Scheunemann, L., Plaças, P.-Y. & Preat, T. Two independent mushroom body output circuits retrieve the six discrete components of *Drosophila* aversive memory. *Cell Reports* **11**, 1280–1292 (2015).
- Hige, T., Aso, Y., Modi, M. N., Rubin, G. M., Turner, G. C. Heterosynaptic plasticity underlies aversive olfactory learning in *Drosophila*. *Neuron* **88**, 985–998 (2015).
- Perisse, E. *et al.* Aversive learning and appetitive motivation toggle feed-forward inhibition in the *Drosophila* mushroom body. *Neuron* **90**, 1086–1099 (2016).
- Liu, X. & Davis, R. L. The GABAergic anterior paired lateral neuron suppresses and is suppressed by olfactory learning. *Nat. Neurosci.* **12**, 53–59 (2009).
- Masuda-Nakagawa, L. M., Ito, K., Awasaki, T. & O’Kane, C. J. A single GABAergic neuron mediates feedback of odor-evoked signals in the mushroom body of larval *Drosophila*. *Front. Neural Circuits* **8**, 35 (2014).
- Honegger, K. S., Campbell, R. A. & Turner, G. C. Cellular-resolution population imaging reveals robust sparse coding in the *Drosophila* mushroom body. *J. Neurosci.* **31**, 11772–11785 (2011).
- Gruntman, E. & Turner, G. C. Integration of the olfactory code across dendritic claws of single mushroom body neurons. *Nat. Neurosci.* **16**, 1821–1829 (2013).
- Litwin-Kumar, A., Harris, K. D., Axel, R., Sompolinsky, H. & Abbott, L. F. Optimal degrees of synaptic connectivity. *Neuron* **93**, 1153–1164.e7 (2017).
- Papadopoulou, M., Cassenaer, S., Nowotny, T. & Laurent, G. Normalization for sparse encoding of odors by a wide-field interneuron. *Science* **332**, 721–725 (2011).

35. Lin, A. C., Bygrave, A. M., de Calignon, A., Lee, T. & Miesenböck, G. Sparse, decorrelated odor coding in the mushroom body enhances learned odor discrimination. *Nat. Neurosci.* **17**, 559–568 (2014).
36. Barnstedt, O. *et al.* Memory-relevant mushroom body output synapses are cholinergic. *Neuron* **89**, 1237–1247 (2016).
37. Mishra, D., Louis, M. & Gerber, B. Adaptive adjustment of the generalization-discrimination balance in larval *Drosophila*. *J. Neurogenet.* **24**, 168–175 (2010).
38. Cassenaer, S. & Laurent, G. Conditional modulation of spike-timing-dependent plasticity for olfactory learning. *Nature* **482**, 47–52 (2012).
39. Takemura, S.-y., *et al.* A connectome of a learning and memory center in the adult *Drosophila* brain. *eLife* **6**, e26975 (2017).
40. Aso, Y., *et al.* Mushroom body output neurons encode valence and guide memory-based action selection in *Drosophila*. *eLife* **3**, e04580 (2014).
41. Aso, Y. & Rubin, G. D. Dopaminergic neurons write and update memories with cell-type-specific rules. *eLife* **5**, e16135 (2016).
42. Schroll, C. *et al.* Light-induced activation of distinct modulatory neurons triggers appetitive or aversive learning in *Drosophila* larvae. *Curr. Biol.* **16**, 1741–1747 (2006).
43. Perisse, E., *et al.* Different Kenyon cell populations drive learned approach and avoidance in *Drosophila*. *Neuron* **79**, 945–956 (2013).
44. Krashes, M. J., *et al.* A neural circuit mechanism integrating motivational state with memory expression in *Drosophila*. *Cell* **139**, 416–427 (2009).
45. Lewis, L. P. *et al.* A higher brain circuit for immediate integration of conflicting sensory information in *Drosophila*. *Curr. Biol.* **25**, 2203–2214 (2015).
46. Liu, W. W. & Wilson, R. I. Glutamate is an inhibitory neurotransmitter in the *Drosophila* olfactory system. *Proc. Natl Acad. Sci. USA* **110**, 10294–10299 (2013).
47. Riemensperger, T., Völler, T., Stock, P., Buchner, E. & Fiala, A. Punishment prediction by dopaminergic neurons in *Drosophila*. *Curr. Biol.* **15**, 1953–1960 (2005).
48. Mao, Z. & Davis, R. L. Eight different types of dopaminergic neurons innervate the *Drosophila* mushroom body neuropil: anatomical and physiological heterogeneity. *Front. Neural Circuits* **3**, 5 (2009).
49. Schultz, W. Neuronal reward and decision signals: from theories to data. *Physiol. Rev.* **95**, 853–951 (2015).
50. Lorenz, K. in *Les Prix Nobel* (ed. Odelberg, W.) (Nobel Foundation, 1973).

Supplementary Information is available in the online version of the paper.

Acknowledgements We thank A. Khandelwal, J. Lovick, J. Valdes-Aleman, I. Larderet, V. Hartenstein, A. Fushiki, B. Afonso, P. Schlegel and M. Berck for reconstructing 31% of arbor cable and 19% of synapses. We thank R. Axel, G. M. Rubin and Y. Aso for their comments on the manuscript. A.L.-K. was supported by National Institutes of Health grant number F32DC014387. A.L.-K. and L.F.A. were supported by the Simons Collaboration on the Global Brain. L.F.A. was also supported by the Gatsby, Mathers, and Kavli Foundations. C.E.P. and Y.P. were supported by the Defense Advanced Research Projects Agency XDATA program (Air Force Research Laboratory contract FA8750-12-2-0303) and National Science Foundation BRAIN EAGER award DBI-1451081. K.E. and A.S.T. thank the Deutsche Forschungsgemeinschaft, TH1584/1-1, TH1584/3-1; the Swiss National Science Foundation, 31003A_132812/1; the Baden Württemberg Stiftung; Zukunftskolleg of the University of Konstanz; and Deutscher Akademischer Austauschdienst. B.G. and T.S. thank the Deutsche Forschungsgemeinschaft, CRC 779, GE 1091/4-1; the European Commission, FP7-ICT MINIMAL. We thank the Fly EM Project Team at Howard Hughes Medical Institute (HHMI) Janelia for the gift of the electron microscopy volume, the Janelia Visiting Scientist program, the HHMI visa office, and HHMI Janelia for funding.

Author Contributions K.E., F.L., A.L.-K., B.G., L.F.A., A.S.T., M.Z. and A.C. conceived the project, analysed the data, and wrote the manuscript. K.E., F.L., I.A., C.S.-M., T.S., A.S.T. and A.C. reconstructed neurons. K.E. performed learning experiments. A.L.-K. built the models. J.W.T. contributed GAL4 lines and their imagery. R.D.F. generated electron microscopy image data. A.L.-K., C.S.-M., Y.P. and C.E.P. analysed connectivity patterns. F.L. and A.H. performed immunostainings. C.E. generated functional data.

Author Information Reprints and permissions information is available at www.nature.com/reprints. The authors declare no competing financial interests. Readers are welcome to comment on the online version of the paper. Publisher's note: Springer Nature remains neutral with regard to jurisdictional claims in published maps and institutional affiliations. Correspondence and requests for materials should be addressed to L.F.A. (lfa2103@columbia.edu), A.S.T. (andreas.thum@uni-leipzig.de), M.Z. (zlatim@hhmi.org) or A.C. (cardonaa@hhmi.org).

METHODS

No statistical methods were used to predetermine sample size. The experiments were not randomized. The investigators were not blinded to allocation during experiments and outcome assessment.

Circuit mapping and electron microscopy. We reconstructed neurons and annotated synapses in a single, complete central nervous system from a 6-h-old [*iso*] Canton S $G1 \times w$ [*iso*] 5905 larva acquired with serial section transmission electron microscopy at a resolution of $3.8 \text{ nm} \times 3.8 \text{ nm} \times 50 \text{ nm}$, which was first published in ref. 11 with the detailed sample preparation protocol. Briefly, the central nervous systems of 6-h-old female larvae were dissected and fixed in 2% glutaraldehyde 0.1 M sodium cacodylate buffer (pH 7.4) to which an equal volume of 2% OsO₄ in the same buffer was added, and microwaved at 350-W, 375-W and 400-W pulses for 30 s each, separated by 60-s pauses, and followed by another round of microwaving but with 1% OsO₄ solution in the same buffer. Then samples were stained *en bloc* with 1% uranyl acetate in water by microwave at 350 W for $3 \times 3 \times 30$ s with 60-s pauses. Samples were dehydrated in an ethanol series, then transferred to propylene oxide and infiltrated and embedded with EPON resin. After sectioning the volume with a Leica UC6 ultramicrotome, sections were imaged semi-automatically with Legikon⁵¹ driving an FEI T20 transmission electron microscope (Hillsboro), and then assembled with TrakEM2 (ref. 52) using the elastic method⁵³.

To map the wiring diagram, we used the Web-based software CATMAID⁵⁴, updated with a novel suite of neuron skeletonization and analysis tools⁵⁵, and applied the iterative reconstruction method⁵⁵. All annotated synapses in this wiring diagram fulfilled the four following criteria of mature synapses^{11,55}: (1) there was a clearly visible T-bar or ribbon; (2) there were multiple vesicles immediately adjacent to the T-bar or ribbon; (3) there was a cleft between the presynaptic and the postsynaptic neurites, visible as a dark–light–dark parallel line; (4) there were postsynaptic densities, visible as black streaks hanging from the postsynaptic membrane.

In this study, we validated the reconstructions as previously described^{11,55}, a method successfully used in multiple studies^{11,55–60}. Briefly, in *Drosophila*, as in other insects, the gross morphology of many neurons is stereotyped and individual neurons are uniquely identifiable on the basis of morphology^{61–63}. Furthermore, the nervous system in insects is largely bilaterally symmetrical and homologous neurons are reproducibly found on the left and the right side of the animal. We therefore validated MBON, DAN, OAN, MBIN, APL, and PN neuron reconstructions by independently reconstructing synaptic partners of homologous neurons on the left and right sides of the nervous system. By randomly re-reviewing annotated synapses and terminal arbors in our dataset, we estimated the false positive rate of synaptic contact detection to be 0.0167 (1 error per 60 synaptic contacts). Assuming the false positives were uncorrelated, for an n -synapse connection the probability that all n were wrong (and thus that the entire connection was a false positive) occurred at a rate of 0.0167^{*n*}. Thus, the probability that a connection was false positive reduced dramatically with the number of synaptic connections contributing to that connection. Even for $n = 2$ synapse connections, the probability that the connection was not true was 0.00028 (once in every 3,586 two-synapse connections) and we called connections with two or more connections ‘reliable’ connections. See refs 11, 55 for more details.

Identification of PNs. The olfactory PNs from this same electron microscopy volume were previously traced and identified¹², with each olfactory glomerulus being innervated by exactly one single uniglomerular PN in the larva⁶⁴. To identify the photosensory and thermosensory PNs connected to KCs, we identified all neurons downstream of 12 photosensory neurons⁶⁵ in the left and right brain hemispheres and all neurons downstream of three previously characterized cold-sensing neurons, expressed in the 11F02-GAL4 line⁶⁶.

Learning in first-instar larvae with a substitution experiment. Learning experiments were performed as described in refs 8, 10, 42, 67. The fly strain *PGMR58E02-GAL4attP2* (Bloomington Stock Center number 41347) and the *attP2* control strain were crossed to *P20XUAS-IVS-CsChrimson.mVenusattP18* (Bloomington Stock Center number 55134). Flies were reared at 25 °C in darkness on 4% agarose with a yeast and water paste including retinal in a 0.5 mM final concentration. First-instar feeding-stage larvae in groups of 30 individuals were placed on plates filled with 4% agarose and the odour ethyl-acetate (100-times diluted in distilled water) was presented on filter papers located on the lid. Larvae were exposed to constant red light (630 nm, power $350 \mu\text{W cm}^{-2}$) during this odour presentation for 3 min. Subsequently larvae were transferred to a new plate and no odour was presented in the dark for 3 min. This paired training cycle was repeated twice. We also performed the unpaired experiment (odour presentation in the dark and red light without odour) with another group of 30 naive larvae. After a 5-min test with odour presentation on one side of the lid, larvae were counted on the side of the odour, no odour, and a 1 cm area in the middle of the plate. Preference and performance indices were calculated as in refs 8, 67: that is, for both the paired

and unpaired, the number of larvae on the no-odour side were subtracted from the number of larvae on the odour side, and the result was divided by the total number of larvae on the plate (including those in the middle). The performance index was half of the value for the paired minus the unpaired preference scores.

Random models of PN-to-KC connectivity. To generate random PN-to-KC models, individual PN connection probabilities were computed as the number of multi-claw KCs contacted divided by the total number of connections onto multi-claw KCs. Probabilities were computed separately for the two hemispheres. To generate the random networks in Fig. 2a, we assumed that PN-to-KC connections were formed independently according to these probabilities. We then iteratively generated KCs until the number of multi-claw KCs matched the number found in the reconstruction. To compare dimension and classification performance for random networks with varying degrees of connectivity (Fig. 2c), we scaled the individual PN connection probabilities so that, on average, each KC received between one and ten claws (Fig. 2b, c). In this case, we fixed the total number of KCs (single- and multi-claw) to be equal to the number found in the reconstruction.

To obtain KCs with a specified number of claws (Fig. 2b), PN connections were determined by weighted random sampling using the individual connection probabilities described above. When comparing detailed connectivity statistics with random models (Extended Data Fig. 3), we used this type of sampling to match the KC claw count distribution for the random models to that of the data.

We also evaluated how many random multi-claw KCs would be required to ensure coverage of the subset of PNs that were connected to single-claw KCs. We restricted our analysis to these PNs and iteratively added random multi-claw KCs, with the claw counts distribution determined by the reconstructed connectivity, until each PN was connected to at least one KC. For this analysis, PN connection probabilities were computed using the full PN-to-KC connectivity matrix.

Model of sparse KC responses. We assumed that the activity of the i th KC was given by $s_i = [\sum_j J_{ij} x_j - \theta_i]_+$, where $[\cdot]_+$ denotes rectification, J is the matrix of PN-to-KC connections, x_j is the activity of the j th PN, and θ_i is the KC activity threshold. Simulated odour-evoked PN activity was generated by sampling the value of each x_j independently from a rectified unit Gaussian distribution. The value of θ_i was adjusted so that each KC fired for a fraction $f = 0.05$ of odours. The entries of J were either the synapse counts from the reconstructed data or, for the case of random connectivity, chosen in the manner of the previous section with a weight sampled randomly from the distribution of PN-to-multi-claw-KC synaptic contact numbers found in the reconstruction.

To assess classification performance (Fig. 2b, c), the KC responses to eight odours were evaluated (ten odours were used when simulating the adult MB). Odour responses again consisted of rectified unit Gaussian random variables, but corrupted by Gaussian noise with standard deviation 0.2. A maximum-margin classifier was trained to separate the odours into two categories to which they were randomly assigned, and the error rate was assessed when classifying odours with different noise realizations. Dimension (Fig. 2f) was assessed by estimating the KC covariance matrix $C_{ij} = \langle (z_i - \langle z_i \rangle)(z_j - \langle z_j \rangle) \rangle$, where z_i is the z -scored activity of neuron i , using 1,000 random simulated odours. We then computed $\text{dim} = (\sum_i \lambda_i)^2 / \sum_i \lambda_i^2$, where $\{\lambda_i\}$ are the eigenvalues of C (ref. 33).

To implement recurrence, we modified the model so that the activity of the i th KC was given by $s_i(t) = \Theta(\sum_j J_{ij} x_j + \sum_k J_{ik}^{\text{rec}} s_k(t-1) - \theta_i)$, where J_{ik}^{rec} is a matrix of recurrent KC-to-KC interactions and t is the timestep. J_{ik}^{rec} is equal to $\alpha_1 J_{ik}^{\text{KC} \rightarrow \text{KC}} + \alpha_2 J_{ik}^{\text{APL}}$, where $J_{ik}^{\text{KC} \rightarrow \text{KC}}$ was determined by the KC-to-KC synapse counts (either dendro-dendritic only or both dendro-dendritic and axo-axonic) and $J_{ik}^{\text{APL}} \propto c_i^{\text{APL} \rightarrow \text{KC}} c_k^{\text{KC} \rightarrow \text{APL}}$, with $c_i^{\text{APL} \rightarrow \text{KC}}$ representing the number of APL synapses onto the i th KC and $c_k^{\text{KC} \rightarrow \text{APL}}$ representing the number of synapses onto APL from the k th KC. J_{ik}^{APL} was scaled so that the average of its entries equalled that of J . The scalar $\alpha_1 = 0.33$ was chosen so that the strength of KC-to-KC and PN-to-KC connections were comparable, while $\alpha_2 = 0.05$ represents the gain of the APL neuron. A single randomly chosen KC was updated on each timestep, with the number of timesteps equal to five times the number of KCs. We also modelled facilitatory KC-to-KC interactions by assuming KC-to-KC connections only depolarized the postsynaptic neuron when it was already above threshold.

Immunostaining. Third-instar larvae were put on ice and dissected in PBS. For all antibodies, brains were fixed in 3.6% formaldehyde (Merck) in PBS for 30 min except anti-dVGlut, which required Bouin's fixation⁶⁸. After several rinses in PBT (PBS with 1% or 3% Triton X-100; Sigma-Aldrich), brains were blocked with 5% normal goat serum (Vector Laboratories) in PBT and incubated for at least 24 h with primary antibodies at 4 °C. Before application of the secondary antibodies for at least 24 h at 4 °C or for 2 h at room temperature, brains were washed several times with PBT. After that, brains were again washed with PBT, mounted in Vectashield (Vector Laboratories), and stored at 4 °C in darkness. Images were taken with a Zeiss LSM 710M confocal microscope. The resulting image stacks were projected and analysed with the image processing software Fiji⁶⁹. Contrast

and brightness adjustment, rotation, and arrangement of images were performed in Adobe Photoshop (Adobe Systems).

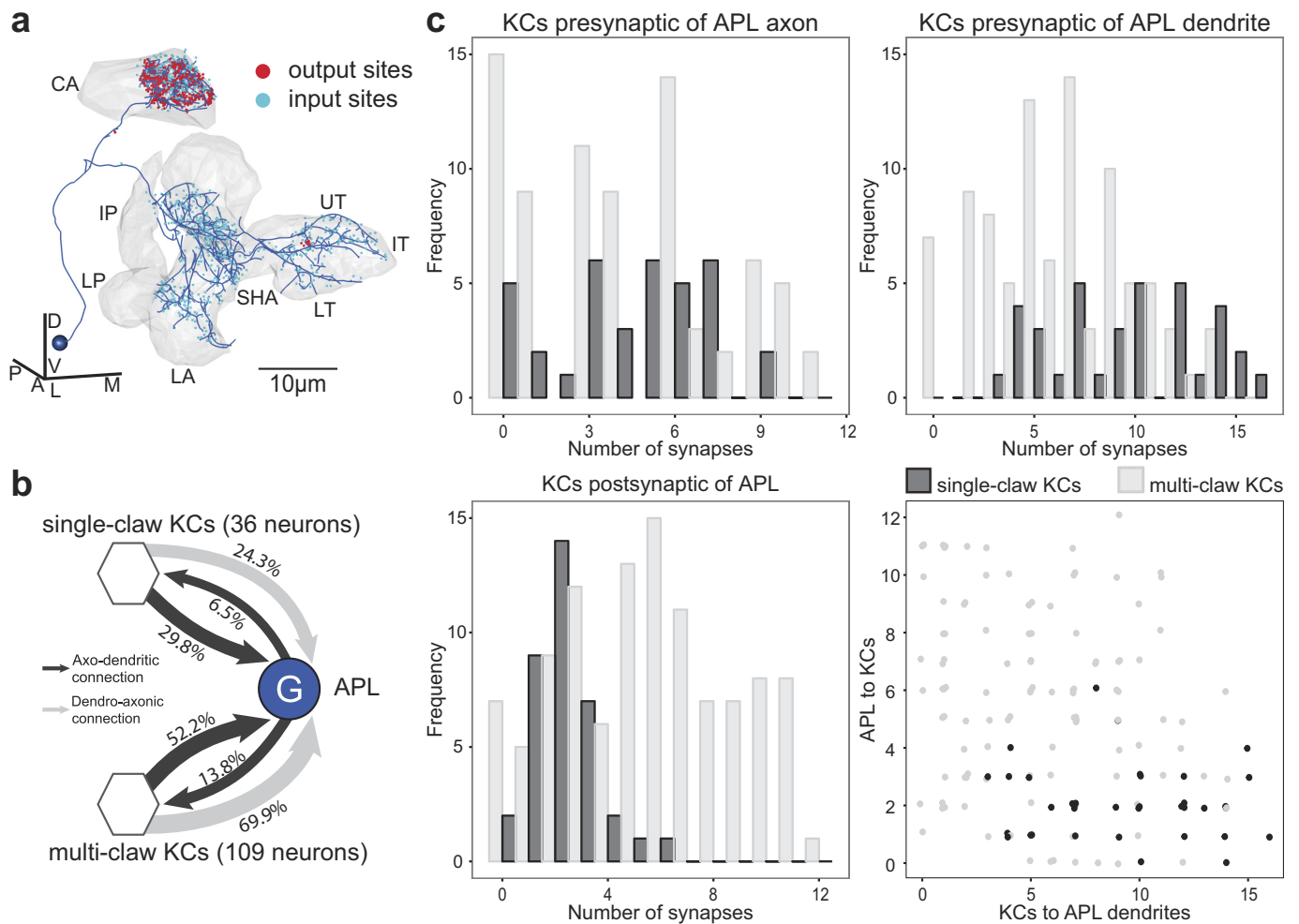
Antibodies. Brains were stained with the following primary antibodies: polyclonal goat anti-GFP fused with FITC (1:1,000, Abcam, ab6662), polyclonal rabbit anti-GFP (1:1,000, Molecular Probes, A6455), polyclonal chicken anti-GFP (1:1,000, Abcam, ab13970), monoclonal mouse anti-TH (1:500, ImmunoStar, 22941), polyclonal rabbit anti-TDC2 (1:200, Covalab, pab0822-P), monoclonal mouse anti-ChAT (1:150, Developmental Studies Hybridoma Bank, ChaT4B1), polyclonal rabbit anti-GABA (1:500, Sigma, A2052), and rabbit anti-dVGlut (1:5,000)⁷⁰ for identifying GFP-positive, dopaminergic, octopaminergic, cholinergic, GABAergic, and glutamatergic neurons. The following secondary antibodies were used: polyclonal goat anti-chicken Alexa Fluor 488 (1:200, Molecular Probes, A11039), polyclonal goat anti-rabbit Alexa Fluor 488 (1:200, Molecular Probes, A11008), polyclonal goat anti-rabbit Alexa Fluor 568 (1:200, Molecular Probes, A11011), polyclonal goat anti-rabbit Cy5 (1:200, Molecular Probes, A10523), polyclonal goat anti-mouse Alexa Fluor 647 (1:200, Molecular Probes, A21235), and polyclonal goat anti-rabbit Alexa Fluor 647 (1:200, Molecular Probes, A21245).

Identifying GAL4 lines that drive expression in MB-related neurons. To identify GAL4 lines (listed in Supplementary Table 3) that drove expression in specific MB-related neurons, we performed single-cell FLP-out experiments (for FLP-out methodology see refs 11, 71) of many candidate GAL4 lines⁷². We generated high-resolution confocal image stacks of the projection patterns of individual MBONs/DANs/OANs (multiple examples per cell type), which allowed their identification. Most MBONs/DANs/OANs were uniquely identifiable on the basis of the dendritic and axonal projection patterns (which MB compartment they projected to and the shape of input or output arbor outside the MB). These were also compared with previously reported single-cell FLP-outs of dopaminergic and octopaminergic neurons in the larva^{8,9,73–75}. Some compartments were innervated by an indistinguishable pair of MBONs or MBINs.

Estimating the birth order of KCs. KCs arise from four neuroblasts per hemisphere that divide continuously from the embryonic to the late pupal stages^{76,77}. The primary neurite of newborn KCs grows through the centre of the MB peduncle, pushing existing KCs to the surface of the peduncle⁷⁸ (Extended Data Fig. 4h). As new cells are added, their somas remain closer to the neuroblast at the surface of the brain and push away existing somas. The point of entry into the lineage bundle of each KC primary neurite remains as a morphological record of the temporal birth order, with some noise. For every KC, we measured the distance from the point where its primary neurite joined the lineage bundle to a reference point consisting of the point where the neurite of the last KC (potentially the oldest of that lineage) joined the bundle, before the bundle entered the neuropil (Fig. 1f) to form the peduncle together with the other three bundles. This measurement revealed that single-claw KCs are born early in MB development, followed by two-claw KCs, three-claw KCs, and so on (Fig. 1f), with the last-born KCs being immature and expected to develop into multi-claw KCs later in larval life⁷⁹.

Data availability. The electron microscopy volume is available at <http://openconnectome.org/catmaid/>, entitled 'acardona_0111_8'. The coordinates for the skeletons modelling neuronal arbors and for the synapses, and the data tables from which all graphs were made, are in the Supplementary Information. Source data for figures and Extended Data figures are available in the Supplementary Information. Any other data are available from the corresponding authors upon reasonable request.

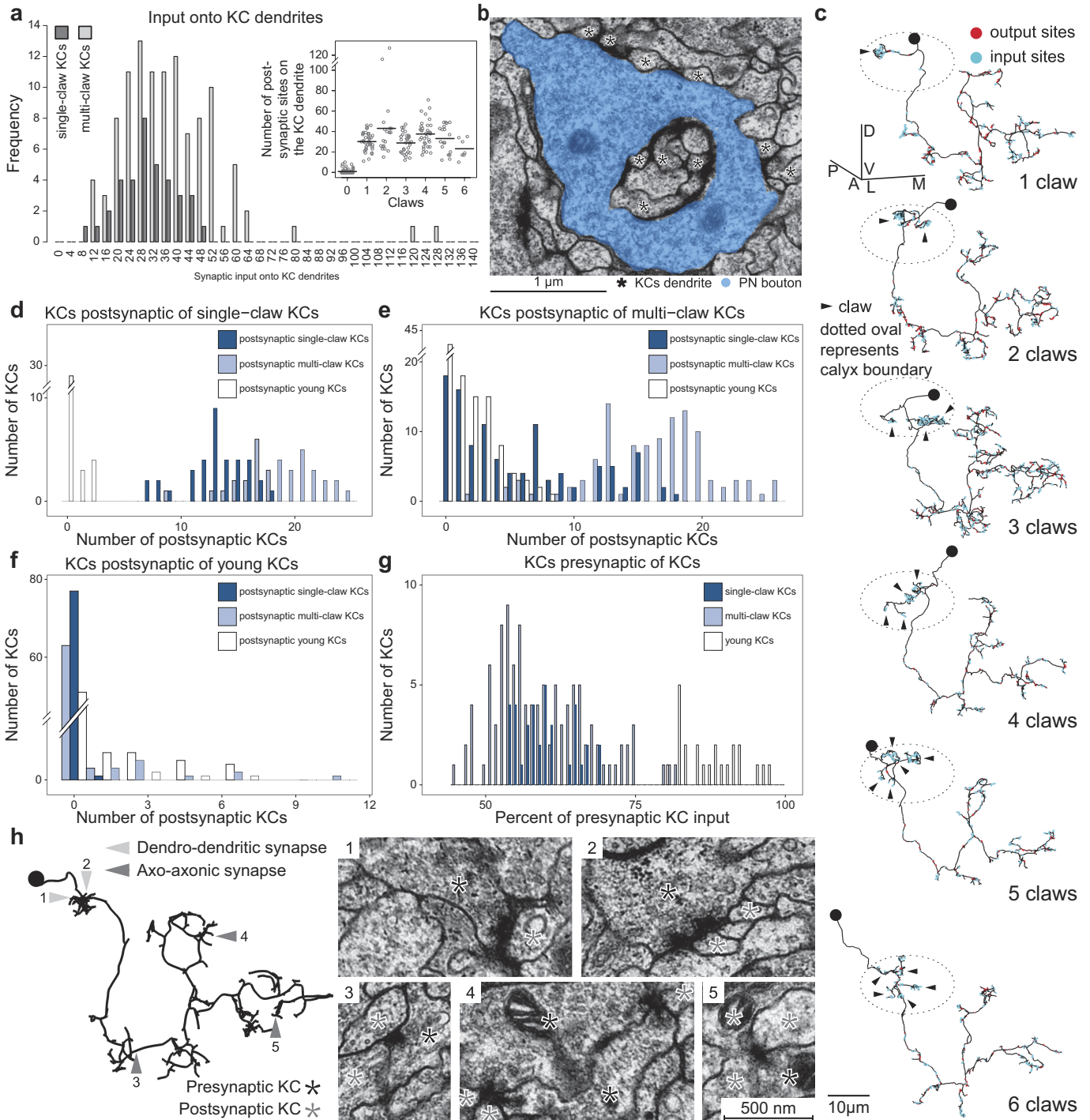
51. Suloway, C. *et al.* Automated molecular microscopy: the new Legimon system. *J. Struct. Biol.* **151**, 41–60 (2005).
52. Cardona, A. *et al.* TrakEM2 software for neural circuit reconstruction. *PLoS ONE* **7**, e38011 (2012).
53. Saalfeld, S., Fetter, R., Cardona, A. & Tomancak, P. Elastic volume reconstruction from series of ultra-thin microscopy sections. *Nat. Methods* **9**, 717–720 (2012).
54. Saalfeld, S., Cardona, A., Hartenstein, V. & Tomancak, P. CATMAID: collaborative annotation toolkit for massive amounts of image data. *Bioinformatics* **25**, 1984–1986 (2009).
55. Schneider-Mizell, C. M., *et al.* Quantitative neuroanatomy for connectomics in *Drosophila*. *eLife* **5**, e12059 (2016).
56. Heckscher, E. S. *et al.* Even-skipped⁺ interneurons are core components of a sensorimotor circuit that maintains left-right symmetric muscle contraction amplitude. *Neuron* **88**, 314–329 (2015).
57. Fushiki, A., *et al.* A circuit mechanism for the propagation of waves of muscle contraction in *Drosophila*. *eLife* **5**, 13253 (2016).
58. Zwart, M. F. *et al.* Selective inhibition mediates the sequential recruitment of motor pools. *Neuron* **91**, 615–628 (2016).
59. Jovanic, T., *et al.* Competitive disinhibition mediates behavioral choice and sequences in *Drosophila*. *Cell* **167**, 858–870 (2016).
60. Schlegel, P. *et al.* Synaptic transmission parallels neuromodulation in a central food-intake circuit. *eLife* **5**, e16799 (2016).
61. Goodman, C. S., Bate, M. & Spitzer, N. C. Embryonic development of identified neurons: origin and transformation of the H cell. *J. Neurosci.* **1**, 94–102 (1981).
62. Bate, M., Goodman, C. S. & Spitzer, N. C. Embryonic development of identified neurons: segment-specific differences in the H cell homologues. *J. Neurosci.* **1**, 103–106 (1981).
63. Costa, M., Manton, J. D., Ostrovsky, A. D., Prohaska, S. & Jefferis, G. S. NBLAST: Rapid, sensitive comparison of neuronal structure and construction of neuron family databases. *Neuron* **91**, 293–311 (2016).
64. Ramaekers, A. *et al.* Glomerular maps without cellular redundancy at successive levels of the *Drosophila* larval olfactory circuit. *Curr. Biol.* **15**, 982–992 (2005).
65. Larderet, I. *et al.* Organization of the *Drosophila* larval visual circuit. Preprint at <https://doi.org/10.1101/133686> (2017).
66. Klein, M. *et al.* Sensory determinants of behavioral dynamics in *Drosophila* thermotaxis. *Proc. Natl Acad. Sci. USA* **112**, E220–E229 (2015).
67. Saumweber, T., Husse, J. & Gerber, B. Innate attractiveness and associative learnability of odors can be dissociated in larval *Drosophila*. *Chem. Senses* **36**, 223–235 (2011).
68. Drobysheva, D. *et al.* An optimized method for histological detection of dopaminergic neurons in *Drosophila melanogaster*. *J. Histochem. Cytochem.* **56**, 1049–1063 (2008).
69. Schindelin, J. *et al.* Fiji: an open-source platform for biological-image analysis. *Nat. Methods* **9**, 676–682 (2012).
70. Daniels, R. W. *et al.* Increased expression of the *Drosophila* vesicular glutamate transporter leads to excess glutamate release and a compensatory decrease in quantal content. *J. Neurosci.* **24**, 10466–10474 (2004).
71. Nern, A., Pfeiffer, B. D. & Rubin, G. M. Optimized tools for multicolor stochastic labeling reveal diverse stereotyped cell arrangements in the fly visual system. *Proc. Natl Acad. Sci. USA* **112**, E2967–E2976 (2015).
72. Li, H.-H. *et al.* A GAL4 Driver resource for developmental and behavioral studies on the larval CNS of *Drosophila*. *Cell Reports* **8**, 897–908 (2014).
73. Selcho, M., Pauls, D., Han, K.-A., Stocker, R. F. & Thum, A. S. The role of dopamine in *Drosophila* larval classical olfactory conditioning. *PLoS ONE* **4**, e5897 (2009).
74. Selcho, M., Pauls, D., Huser, A., Stocker, R. F. & Thum, A. S. Characterization of the octopaminergic and tyraminergergic neurons in the central brain of *Drosophila* larvae. *J. Comp. Neurol.* **522**, 3485–3500 (2014).
75. Slater, G., Levy, P., Chan, K. L. & Larsen, C. A central neural pathway controlling odor tracking in *Drosophila*. *J. Neurosci.* **35**, 1831–1848 (2015).
76. Ito, K. & Hotta, Y. Proliferation pattern of postembryonic neuroblasts in the brain of *Drosophila melanogaster*. *Dev. Biol.* **149**, 134–148 (1992).
77. Kunz, T., Kraft, K. F., Technau, G. M. & Urbach, R. Origin of *Drosophila* mushroom body neuroblasts and generation of divergent embryonic lineages. *Development* **139**, 2510–2522 (2012).
78. Kurusu, M. *et al.* Embryonic and larval development of the *Drosophila* mushroom bodies: concentric layer subdivisions and the role of fasciclin II. *Development* **129**, 409–419 (2002).
79. Lee, T., Lee, A. & Luo, L. Development of the *Drosophila* mushroom bodies: sequential generation of three distinct types of neurons from a neuroblast. *Development* **126**, 4065–4076 (1999).
80. Blondel, V. *et al.* Fast unfolding of communities in large networks. *J. Stat. Mech.* **2008**, P10008 (2008).



Extended Data Figure 1 | Connectivity of the larval APL neuron.

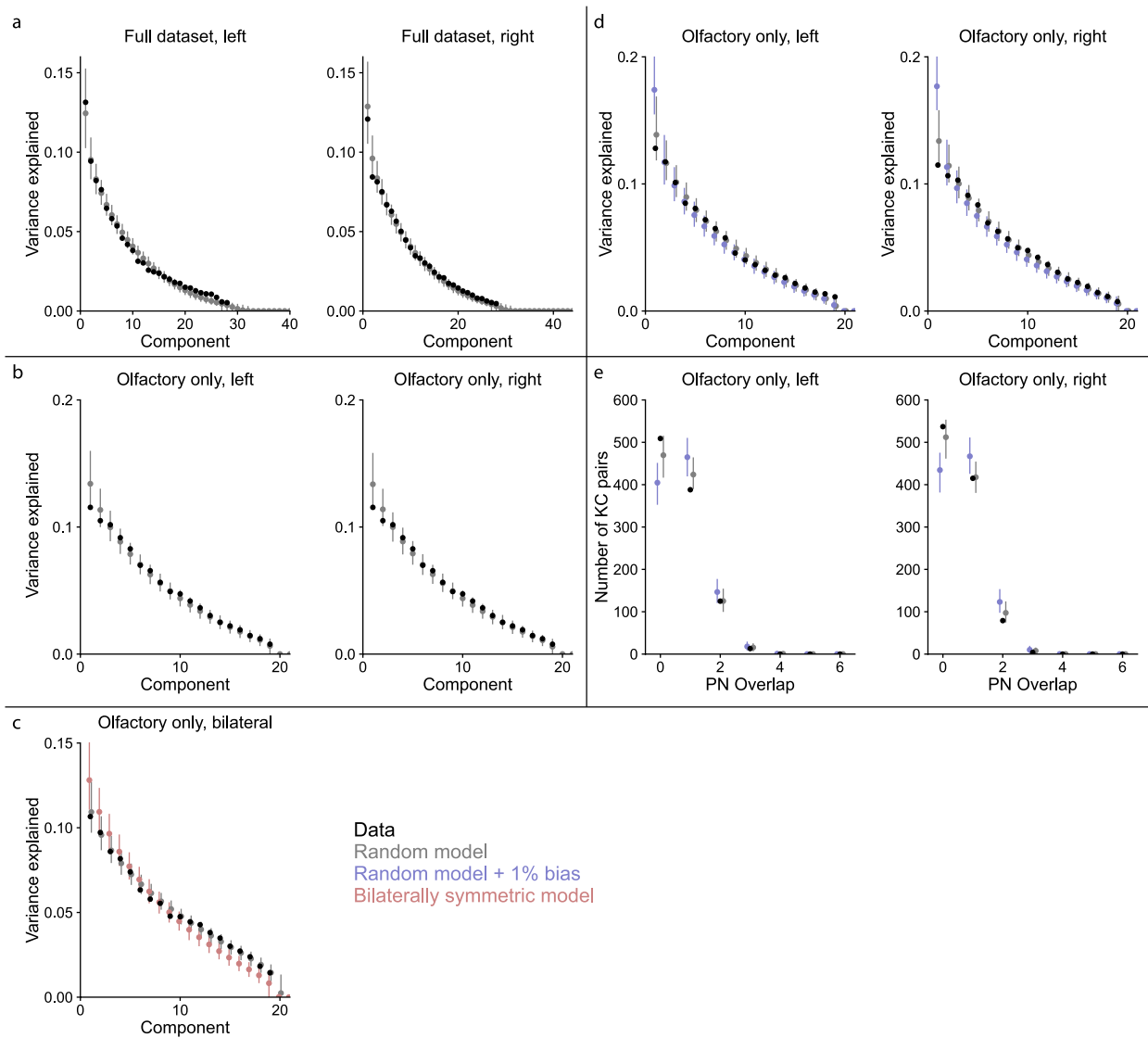
a, Morphology of the right-hemisphere larval APL neuron. While APL dendrites are postsynaptic to the KCs in LA, LVL, IVL, and all medial lobe compartments, its axon is both post- and presynaptic to the MB calyx. Presynaptic sites in red and postsynaptic sites in blue. **b**, APL connectivity with KC types. Connections are displayed as fractions of input onto the receiving neurons. APL forms more axo-dendritic connections with multi-claw than with single-claw KCs. All mature KCs connect to APL

on its dendrite as well as on its axon. **c**, Strength of synaptic connections between KCs and the APL neuron for single-claw and multi-claw KCs separately. While single-claw KCs have a higher synapse count connecting to the APL dendrites than multi-claw KCs, both groups of KCs project a similar number of synapses to the APL axon. In the calyx, APL makes more synapses onto multi-claw than onto single-claw KCs. In the lobes, single-claw KCs make more synapses with APL pre- than postsynaptically.



Extended Data Figure 2 | Input onto KC dendrites and KC-KC connections. **a**, Total synaptic input onto KC dendrites from PNs, the APL neuron, and calyx MBINs for single- and multi-claw KCs from both hemispheres. Inset: sum of the KC postsynaptic sites in the calyx as a function of the number of claws. Grey circles show individual KCs and black line shows the mean. Young KCs that have no claws or only form short branches in the calyx have few postsynaptic sites. Mature KCs forming one to six claws present a similar total amount of postsynaptic sites in the calyx. **b**, A PN bouton (blue) and its associated KC dendritic arborizations. Stars indicate all dendrites of the single-claw KC for this PN. **c**, Prototypical examples of KCs according to the structure of their dendrites, commonly known as 'claws'. In first instar, we define each 'claw' (indicated by arrowheads) as a connection from a PN providing at least 10% of the postsynaptic sites of the KC dendritic arbor. This connectivity-

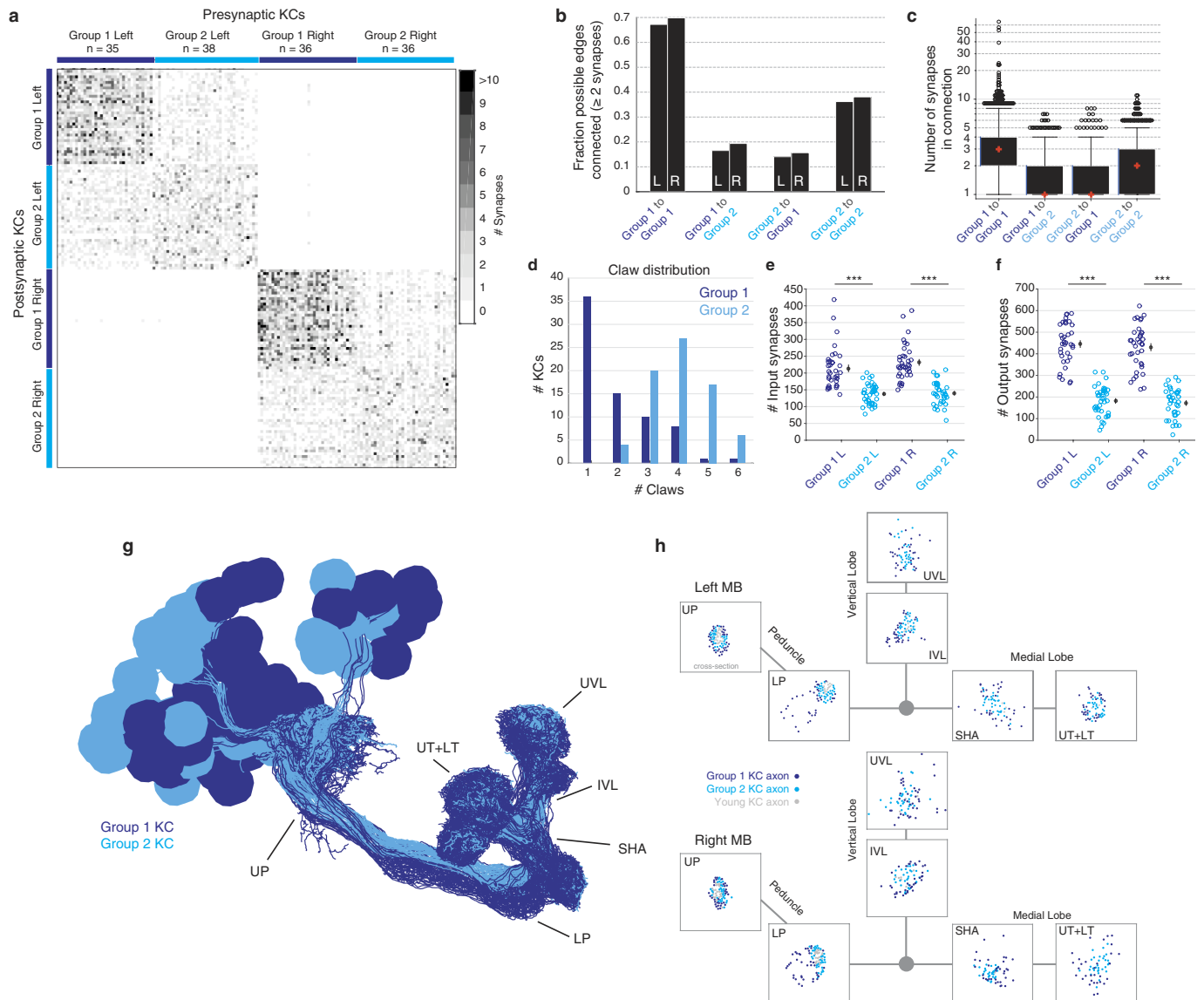
based definition generally agrees with the count of physically separate claw-like dendritic branches that wrap around the axon terminals of the PNs. Single-claw KCs have not yet been described in the adult fly or other insects. **d-g**, Frequency of different numbers of postsynaptic KC-partners of KCs with at least two-synapse connections, plotted separately for three different types of KC. **d**, Postsynaptic partners of single-claw KCs. **e**, Postsynaptic partners of multi-claw KCs. **f**, Postsynaptic partners of young KCs. **g**, KC input onto KCs as a percentage of total KC input. For most KCs, more than 50% of their presynaptic partners are other KCs. **h**, Morphology of an example reconstructed KC (left) and example electron micrographs showing KC-KC synapses (right). Dendro-dendritic connections are in the calyx compartment (1 and 2) and axo-axonic connections are located in the peduncle (3), vertical lobe (4), and medial lobe (5).



Extended Data Figure 3 | Test of structure in PN-to-KC connectivity.

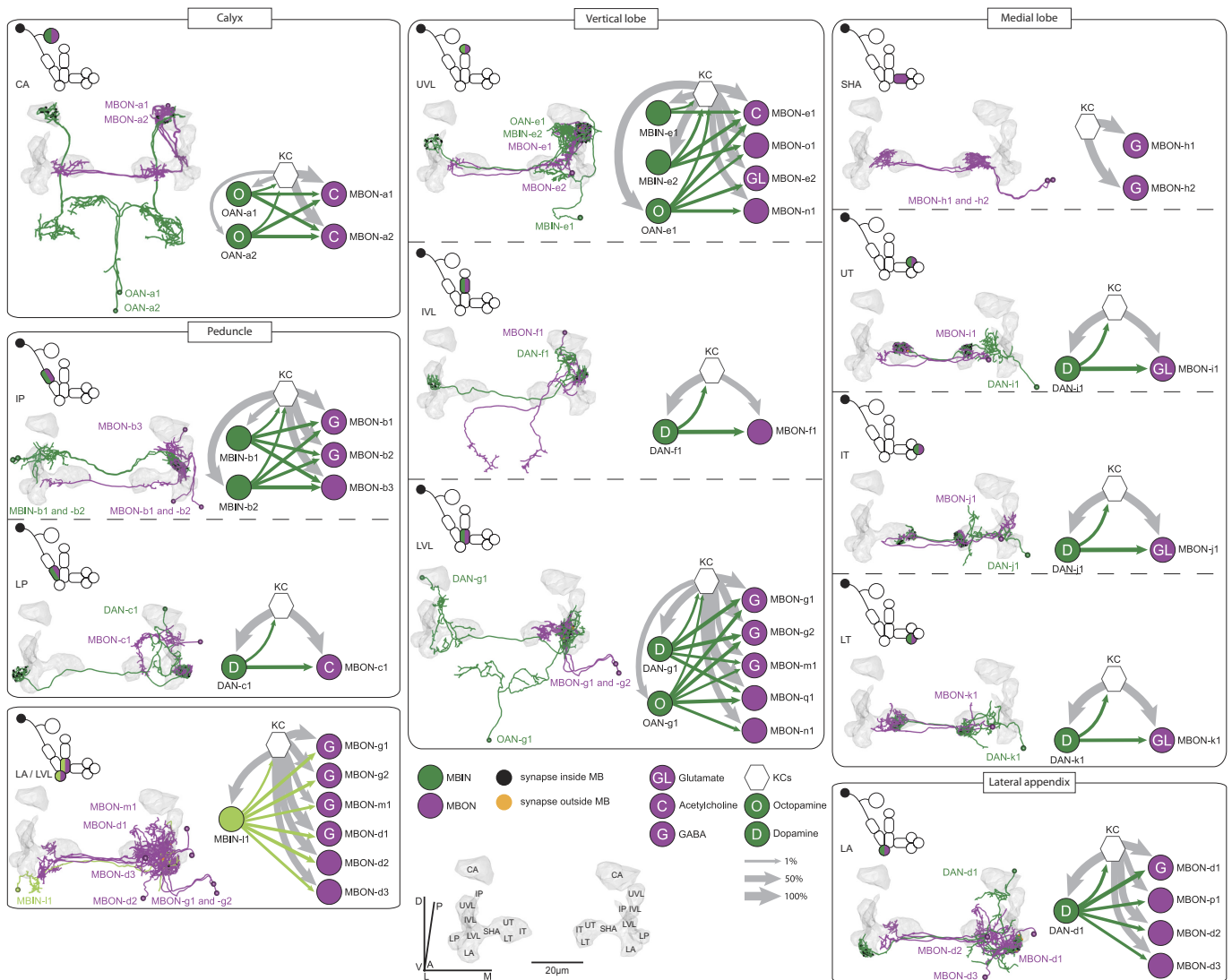
a, We performed principal component analysis on the PN-to-KC connectivity matrices for the left and right hemispheres. The analysis was restricted to multi-claw KCs. The variance explained by each principal component in descending order is compared with that obtained from random models in which KCs sample PNs according to the individual PN connection probabilities (see Methods). Grey circles and bars denote mean and 95% confidence intervals for the variance explained by each principal component of the random connectivity matrices, while the black circles indicate the values obtained from data. Note a small deviation from the random model, probably because of the non-olfactory PNs. **b**, Same as **a** but restricted to connections between olfactory PNs and KCs. **c**, Same as **b** but combining the PN-to-KC connectivity for both hemispheres. The data are compared with a random model in which KCs in each hemisphere sample PNs randomly and independently (grey), and with a bilaterally symmetrical model in which the connectivity is random but duplicated

across the two hemispheres (pink). **d**, To assess the ability of our method to identify structured connectivity, we also generated connectivity matrices in which a weak bias was added (blue). Networks were generated in which PNs were randomly assigned to one of two groups. For each KC, the probabilities of connecting to PNs belonging to one randomly chosen group were increased by 1%, while the probabilities for the other group were decreased by 1% (the baseline probabilities were on average approximately 5%). This procedure was performed independently for each KC and led to networks in which KCs preferentially sampled certain PNs. The data are inconsistent with this model, illustrating that biases of $\sim 1\%$ connection probability can be identified using our methods. **e**, As an independent method to identify structure in the PN-to-KC wiring, we considered the distribution of olfactory PN overlaps for all KC pairs, defined as the number of olfactory PNs from which both KCs received input. This quantity specifically identified biases in the likelihood of KCs to sample similar inputs. As in **b**, no such structure was identified.



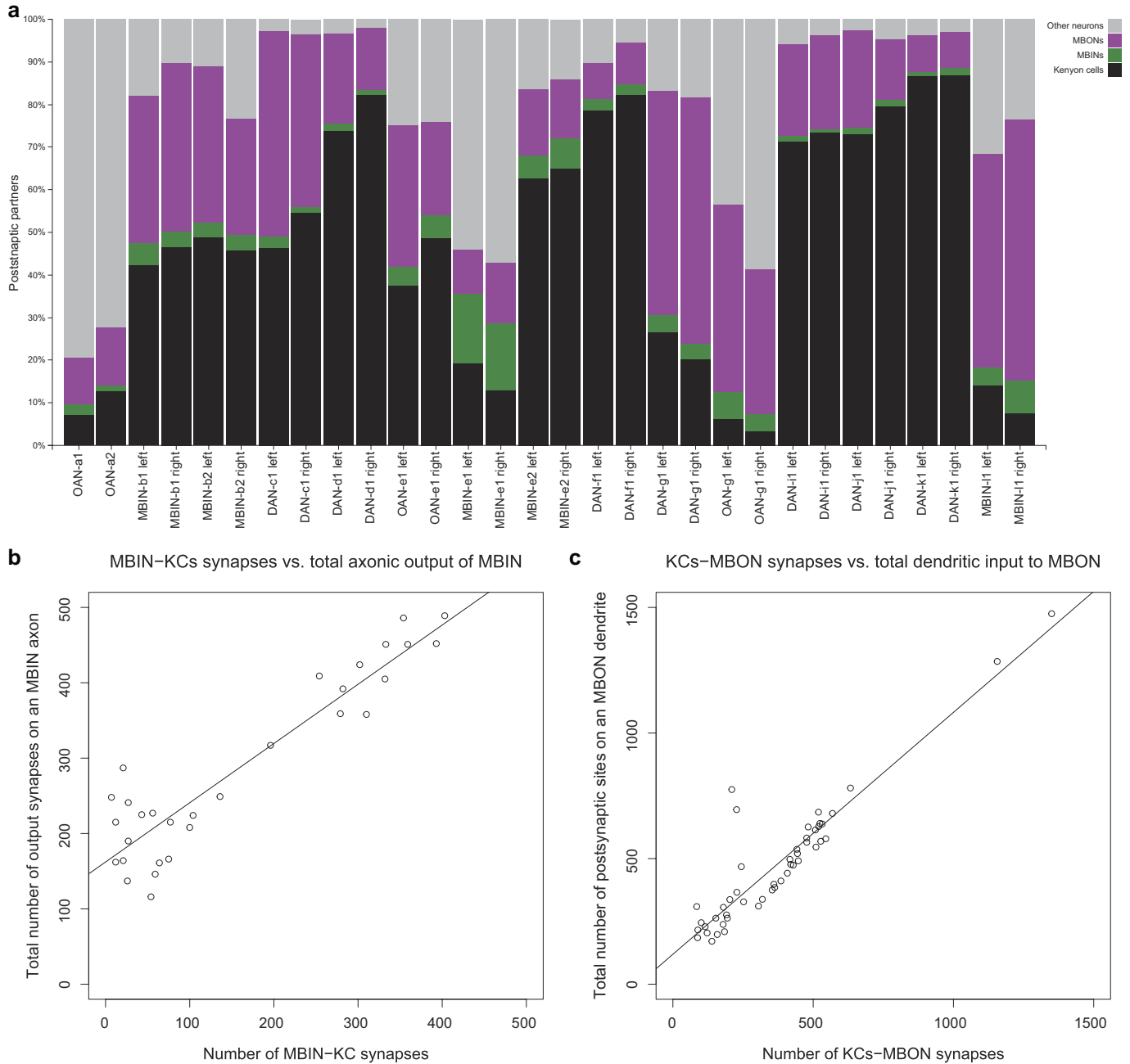
Extended Data Figure 4 | KC–KC clustering. Synaptic connectivity between KCs reveals two communities within the MB. **a**, Heat map representation of the KC–KC network adjacency matrix, sorted by community structure as discovered by the Louvain method⁸⁰, which identifies groups of KCs with more within-group connections than expected by chance. We denote the denser community on each side as ‘Group 1’ and the other community as ‘Group 2’. Number of cells in each group is shown in the column labels. **b**, The number of observed 2+ synapse connections between pairs of KCs within and between groups in the same side of the body, normalized by the total number of all possible such connections (L, left; R, right). **c**, Distribution of number of synapses per edge for connections within and between each group. Boxes indicate interquartile interval, whiskers the 95th percentile, cross indicates median,

outliers shown. **d**, Claw distribution by group (both sides aggregated). Note that all single-claw KCs are in Group 1. **e**, Total number of anatomical input synapses onto Group 1 and Group 2 KCs, including from non-KC sources. Group 1 cells have significantly more inputs than Group 2 cells on each side ($P < 10^{-10}$, *t*-test with Bonferroni correction). **f**, Total number of anatomical output synapses from Group 1 and Group 2 KCs, including synapses onto non-KC targets. Group 1 cells have significantly more outputs than Group 2 cells on each side ($P < 10^{-10}$, *t*-test with Bonferroni correction). **g**, KC anatomy labelled by group for the right MB. Note that both groups of KCs come from each lineage cluster. Labelled spots indicate locations of cross-section views in **h**. **h**, Cross-sections of the two principal axon branches of KCs in the left (above) and right (below) MBs at the locations indicated in **g**. Orientations of each cross-section are arbitrary.



Extended Data Figure 5 | Neurons in the canonical circuit in every MB compartment. Neuronal morphology and connectivity of MBINs and MBONs participating in the canonical circuit motif of each MB compartment (MBINs in green and MBONs in magenta). Neurons connecting to the left-hemisphere MB are displayed in anterior view (right hemisphere has the same morphology, data not shown). Locations of MBINs synapsing on MBONs in a given compartment are shown depending on their location (inside the MB neuropil, black; outside

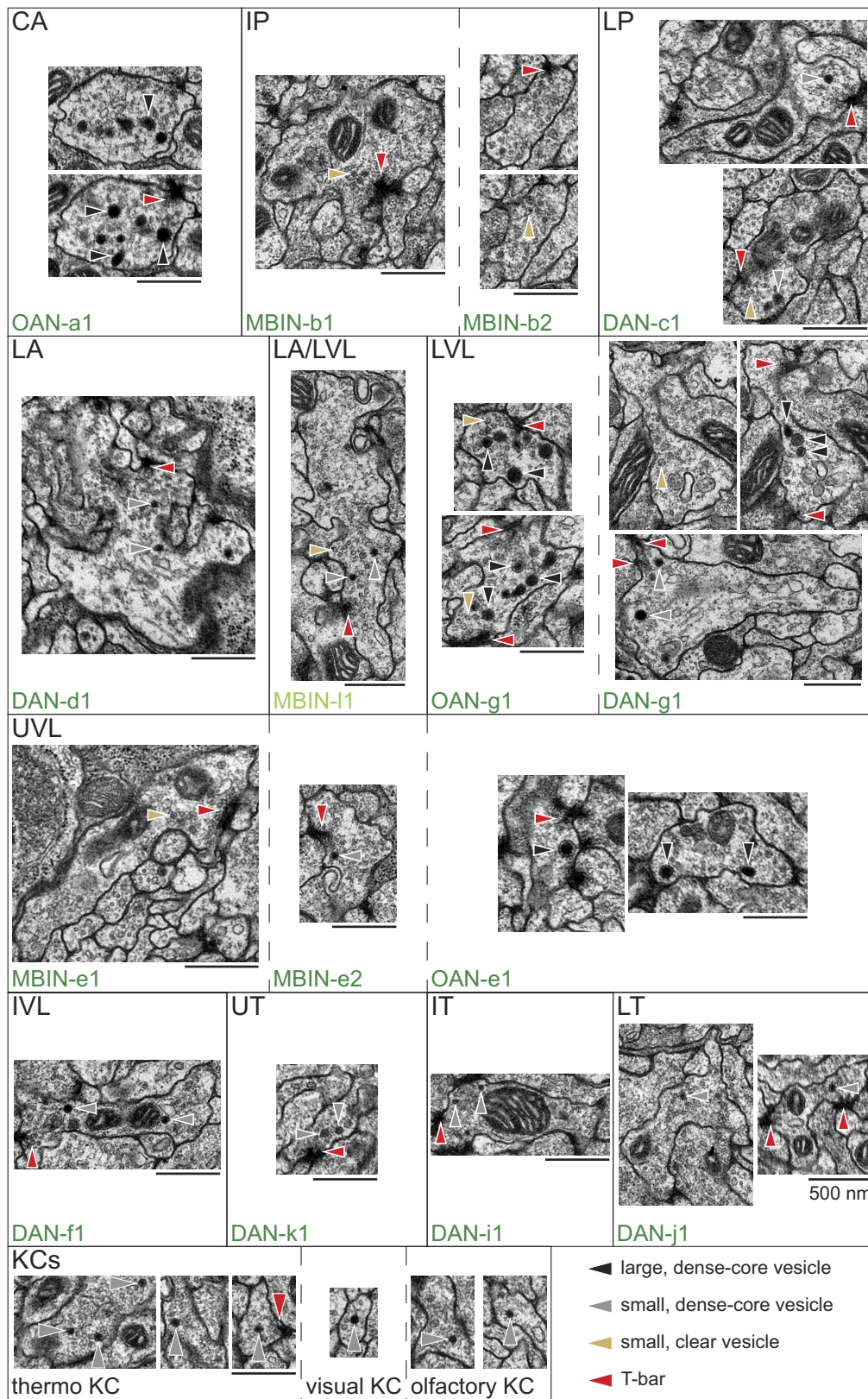
the MB, orange). MBIN axons and MBON dendrites tile the MB into 11 distinct compartments. For each compartment, the MBIN and MBON neurons and their connections as a fraction of total input to the receiving neuron are shown on the right. MBONs are diverse in the neurotransmitter that they release (see legend). All compartments present the canonical circuit motif except for SHA, which does not develop its DAN until later in larval life.



Extended Data Figure 6 | Fractions of postsynaptic inputs by cell type.

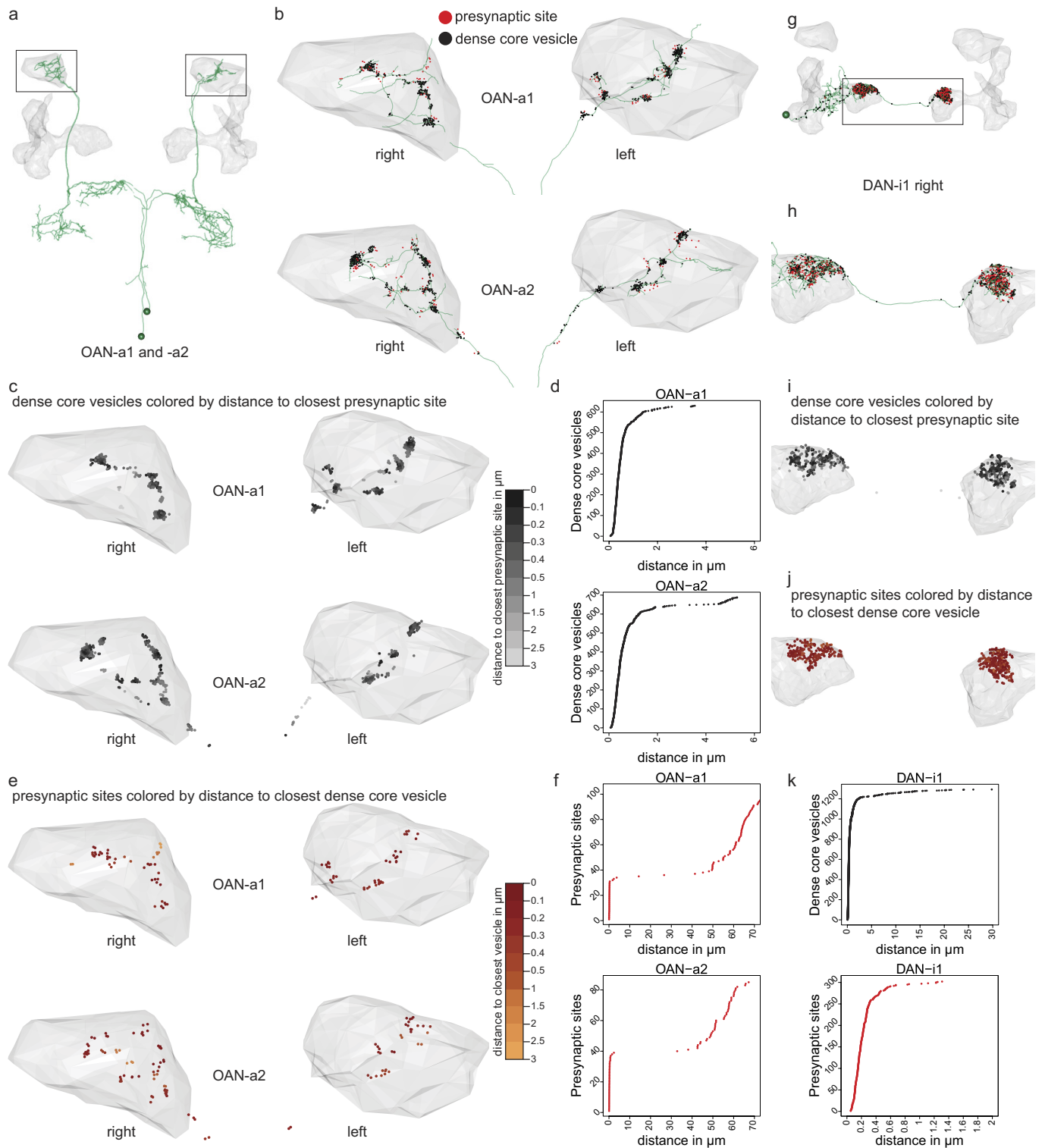
a, Fractions of synaptic output from MBINs onto KCs, other MBINs, MBONs, and other neurons. Some MBINs show a high percentage of connections to MB neurons while others connect with less than 50% of their synapses to MB neurons. **b**, Number of MBIN-KC synapses in relation to the number of total synaptic outputs from MBIN axons,

showing a positive correlation between presynaptic sites on the MBIN axon and synapses dedicated to KC population. **c**, Number of KC-MBON synapses in relation to the number of total synaptic inputs to MBON dendrites, showing a positive correlation between postsynaptic sites on the MBON dendrite and fraction of input from KCs.



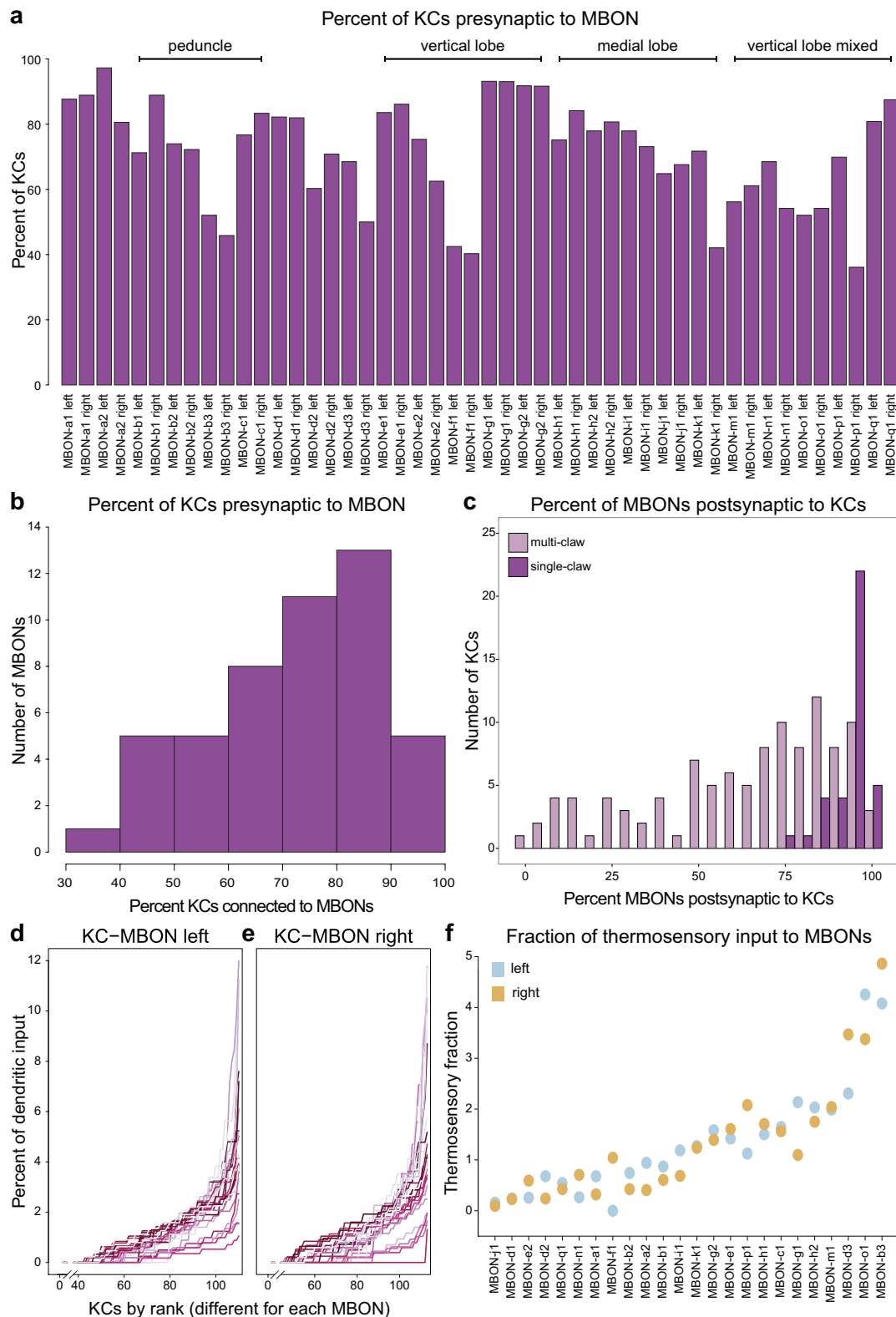
Extended Data Figure 7 | MBIN presynaptic vesicle types. Examples of electron micrographs of MBIN presynaptic sites and vesicles. We found three types of vesicle: large dense-core, small dense-core, and small clear vesicles. Octopaminergic and dopaminergic neurons contain small clear vesicles in addition to other vesicle types. While OANs have all the same type of large dense-core vesicles, DANs show a variety of small dense-core

vesicles. We found small dense-core vesicles in one-third of KCs. Some of these were single-claw, others were multi-claw, some received olfactory input, and others non-olfactory PN input. The largest number of dense-core vesicles was observed in the two thermosensory KCs. Scale bar, 500 nm in all panels.



Extended Data Figure 8 | Dense-core vesicles in OANs and DANs.
a, Morphology of OAN-a1 and -a2 innervating the calyx of both MBs.
b, Location of presynaptic sites (red) and dense-core vesicles (DCVs/ black) along the axon of OAN-a1 and -a2. **c**, DCVs colour-coded by their distance to the closest presynaptic site on the axon of OAN-a1 and -a2. **d**, Distance (in micrometres) of DCVs to the closest presynaptic site sorted by the value for OAN-a1 and -a2. Most DCVs are within 2 μm from a presynaptic site, just a few are further away and appear to be in transit. **e**, Presynaptic sites colour-coded by their distance to the closest DCV on the axon of OAN-a1 and -a2. **f**, Distance (in micrometres) of presynaptic sites to the closest DCV sorted by the value for OAN-a1 and -a2. Half of the presynaptic sites have a DCV associated within 20 μm . Some presynaptic sites have no close DCV associated and are located in the

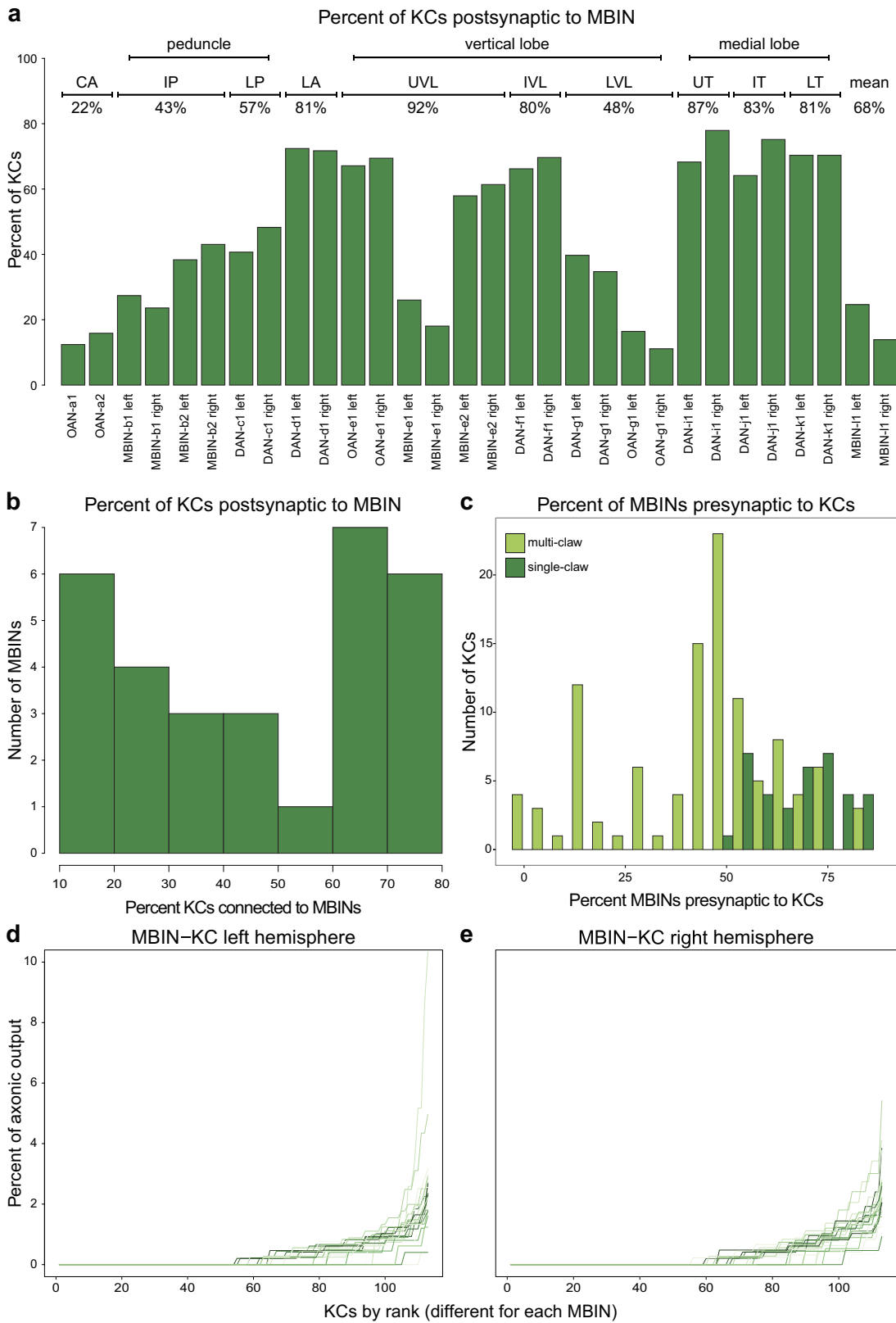
dendrites of OAN-a1 and -a2 (data not shown). **g**, Morphology of DAN-i1 right innervating the upper toe of the MB medial lobe in both hemispheres with the location of presynaptic sites (red) and DCVs (black). **h**, Zoom-in onto the medial lobes from **g**. **i**, DCV colour-coded by their distance to the closest presynaptic site on the axon of DAN-i1 right. **j**, Presynaptic sites colour-coded by their distance to the closest DCV on the axon of DAN-i1 right. **k**, Distance (in micrometres) of DCVs to the closest presynaptic site sorted by the value for DAN-i1 right and left together. Some DCVs are further away from presynaptic sites than 10 μm ; these DCVs are in the dendrites of the DAN (shown in **g**). And distance (in micrometres) of presynaptic sites to the closest DCV sorted by the value for DAN-i1 right and left together. Most of the presynaptic sites have a DCV associated within 1 μm .



Extended Data Figure 9 | KC-to-MBON synaptic connections.

a, Percentage of mature KCs that are presynaptic to a given MBON. **b**, Frequency of the percentage of KCs presynaptic to MBONs (bin width is 10%). **c**, Frequency of the percentage of MBONs each KC connects to for single-claw and multi-claw KCs separately. All single-claw KCs connect with at least 75% of all MBONs present in their own hemisphere. **d**, Percentage of dendritic MBON inputs from individual KCs in the left brain hemisphere. KCs are ranked by their number of synapses to the MBON for each MBON separately (each line represents an MBON). Note the rank order of KCs is different for every MBON. Note also that a few

MBONs receive very strong synaptic input from approximately 20 KCs and less than 3% from the remaining KCs, while most MBONs receive less than 4% of dendritic input from all KCs. **e**, Same as **d**, but for the right brain hemisphere. **f**, Effective strength of thermosensory input to MBONs. The thermosensory fraction is defined as the number of synapses received by an MBON from thermosensory KCs divided by 0.05 times the number of synapses received from all other KCs. The fraction thus represents the relative influence of an input that activates the thermosensory KCs compared with that of a typical stimulus that activates 5% of KCs.



Extended Data Figure 10 | MBIN-to-KC synaptic connections.

a, Percentage of mature KCs that are postsynaptic to a given MBIN. On average, 68% of KCs in a compartment are postsynaptic to at least one MBIN of that compartment. **b**, Frequency of the percentage of KCs postsynaptic to MBINs (bin width is 10%). **c**, Frequency of the percentage of MBINs presynaptic to each KC for single-claw and multi-claw KCs separately. All single-claw KCs receive synaptic input from at least 50% of all MBINs present in their own hemisphere. **d**, Percentage of axonic

outputs from MBINs connecting to individual KCs in the left brain hemisphere. KCs are ranked by their number of synapses they receive from an MBIN for each MBIN separately (each line represents a MBIN). Note the rank order of KCs is different for every MBIN. Note also that a few MBINs connect very strongly to approximately ten KCs and less than 2% to the remaining KCs, while most MBINs dedicate less than 2% of their axonic output to all KCs. **e**, Same as **d**, but for the right brain hemisphere.

Life Sciences Reporting Summary

Nature Research wishes to improve the reproducibility of the work we publish. This form is published with all life science papers and is intended to promote consistency and transparency in reporting. All life sciences submissions use this form; while some list items might not apply to an individual manuscript, all fields must be completed for clarity.

For further information on the points included in this form, see Reporting Life Sciences Research. For further information on Nature Research policies, including our data availability policy, see Authors & Referees and the Editorial Policy Checklist.

Experimental design

1. Sample size

Describe how sample size was determined.

The sample size of 1 was chosen as the minimally interesting and maximally doable within 3 years.

2. Data exclusions

Describe any data exclusions.

No data was excluded.

3. Replication

Describe whether the experimental findings were reliably reproduced.

The nervous system is bilaterally symmetric, therefore we have N=2, although the two samples are not entirely independent.

4. Randomization

Describe how samples/organisms/participants were allocated into experimental groups.

Not applicable.

5. Blinding

Describe whether the investigators were blinded to group allocation during data collection and/or analysis.

Not applicable.

Note: all studies involving animals and/or human research participants must disclose whether blinding and randomization were used.

6. Statistical parameters

For all figures and tables that use statistical methods, confirm that the following items are present in relevant figure legends (or the Methods section if additional space is needed).

n/a Confirmed

- The exact sample size (*n*) for each experimental group/condition, given as a discrete number and unit of measurement (animals, litters, cultures, etc.)
- A description of how samples were collected, noting whether measurements were taken from distinct samples or whether the same sample was measured repeatedly.
- A statement indicating how many times each experiment was replicated
- The statistical test(s) used and whether they are one- or two-sided (note: only common tests should be described solely by name; more complex techniques should be described in the Methods section)
- A description of any assumptions or corrections, such as an adjustment for multiple comparisons
- The test results (e.g. *p* values) given as exact values whenever possible and with confidence intervals noted
- A summary of the descriptive statistics, including central tendency (e.g. median, mean) and variation (e.g. standard deviation, interquartile range)
- Clearly defined error bars

See the web collection on statistics for biologists for further resources and guidance.

Software

Policy information about availability of computer code

7. Software

Describe the software used to analyze the data in this study.

We used primarily the open source software CATMAID (<https://github.com/catmaid/catmaid>) for neuron reconstruction and Matlab and R scripts available upon request.

For all studies, we encourage code deposition in a community repository (e.g. GitHub). Authors must make computer code available to editors and reviewers upon request. The *Nature Methods* guidance for providing algorithms and software for publication may be useful for any submission.

Materials and reagents

Policy information about availability of materials

8. Materials availability

Indicate whether there are restrictions on availability of unique materials or if these materials are only available for distribution by a for-profit company.

We used the same EM volume reported in Ohyama et al. 2015 (Nature) and available at <https://neurodata.io>. There are no restrictions on availability.

9. Antibodies

Describe the antibodies used and how they were validated for use in the system under study (i.e. assay and species).

We used antibodies that were used before in prior publications by the Thum lab. For example in Selcho et al. 2009; Selcho et al. 2012.

10. Eukaryotic cell lines

a. State the source of each eukaryotic cell line used.

Not applicable.

b. Describe the method of cell line authentication used.

Not applicable.

c. Report whether the cell lines were tested for mycoplasma contamination.

Not applicable.

d. If any of the cell lines used in the paper are listed in the database of commonly misidentified cell lines maintained by ICLAC, provide a scientific rationale for their use.

Not applicable.

Animals and human research participants

Policy information about studies involving animals; when reporting animal research, follow the ARRIVE guidelines

11. Description of research animals

Provide details on animals and/or animal-derived materials used in the study.

Drosophila larva, female. Same individual as in Ohyama et al. 2015, Nature.

Policy information about studies involving human research participants

12. Description of human research participants

Describe the covariate-relevant population characteristics of the human research participants.

Not applicable.